Simulating Optical Pumping in the Laser Spectroscopy Experiment at TRIUMF

Julien Refour

Masters of Science

Department of Physics

McGill University

Montreal, Quebec

2017-12-14

Requirements Statement

ACKNOWLEDGEMENTS

In no particular order, I must thank my supervisors: Dr. Matthew Pearson, Dr. Fritz Buchinger and Dr. John Crawford (between the three of which exists a well of endless patience and advice) and Andrea Teigelhoefer, who repeatedly helped me with the theoretical part of this work. Of course, I would like to thank my parents, without whom I may never have had the drive, desire or support to complete this thesis. Finally, thanks must be extended to all the friends that have made Vancouver more of a home than I could ever imagine.

ABSTRACT

Laser spectroscopy is a technique that can be used to probe the electronic structure of atoms/ions. The Collinear Fast Beam Spectroscopy (CFBS) group at TRIUMF uses this technique to probe the hyperfine structure of rare isotopes produced on-site. The hyperfine structure of an atom, which arises from the various interactions between the atom's/ion's electrons and nucleus, can be used to infer properties, such as the spin and mean squared charge radius, of the atom's nucleus. However, the geometry of the experimental set up at TRIUMF allows for the possibility of optical pumping, a process by which the atoms/ions being probed have their electronic ground state distribution changed before the hyperfine structure can be measured. This in turn can change the relative intensities of the hyperfine transitions being measured. Optical pumping depends, mainly, on the power of the laser used to excite the hyperfine transitions being studied. In this work, a statistical model designed to simulate the effects of optical pumping on hyperfine spectra measured at TRIUMFs CFBS experiment. With the goal of simulating the hyperfine spectrum of any atom under investigation, the model is based on the likelihood that an atom/ion reaches the region where the hyperfine spectrum is measured in its original ground state. This likelihood is in turn used the modify the relative intensities of each hyperfine transition. The effects of laser power, the temperature of the atoms/ions, and the distance they must travel before being measured are examined. Additionally, the predictions of the model are compared to previously measured Gallium-69 and Rubidium-87 hyperfine spectra. Discrepancies between the assumed temperature and the temperature predicted by the model were observed in the case of Gallium-69, with a possible resolution being the effects of accelerating the atoms/ions when they

are extracted from a Radio Frequency Quadrupole trap used for bunching. In the case of Rubidium-87, a discrepancy between the expected and measured relative intensity of particular transition is observed. This may be due to an over-estimation of the power delivered to the atoms.

ABRÉGÉ

Un model statistique, construit pour la simulation des effets du pompage optique sur les spectres hyperfines mesurés à TRIUMF, est présenté. Les résultats de ce model, construit sur la probabilité qu'une atome arrive dans la région d'interaction dans son état de repos original, sont comparés avec des spectres mesurés du Gallium-69 et Rubidium-87. Dans le cas du Gallium-69, une différence entre la température assumée et la température calculée a été observée, provenant peut-être des effets des voltages appliqués aux atomes lors de leur extraction et accélération. Pour le Rubidium-87, une différence entre les intensités mesurée et calculés de la transition $F_e = 1 \rightarrow F_g = 2$ a été observée, les origines de laquelle viennent d'une surestimation de l'intensité du laser.

TABLE OF CONTENTS

ACKNOWLEDGEMENTS ii

ABSTRACT iii

ABRÉGÉ v

LIST OF TABLES viii

LIST OF FIGURES ix

1 Introduction 1

2 Laser Spectroscopy at TRIUMF 4

2.1 Radio Frequency Quadrupole (RFQ) Trap 4
2.2 Charge Exchange Cell (CEC) 6
2.3 Light Collection Region (LCR) 7

3 Theory of Laser Spectroscopy 9

3.1 Anatomy of a Hyperfine Spectrum 9
3.1.1 Peak Energies 11
3.1.2 Peak intensities 15
3.1.3 Peak Widths 16
3.2 Spontaneous Emission in Multi-Level Atoms 18
3.2.1 The Dipole Moment 20
3.2.2 Selection Rules 23
3.3 Photon Scattering Rates 24

4 Simulation of Optical Pumping 25

4.1 Optical Pumping as a Modification to the Racah Intensities 28
4.1.1 Interaction Time 28
4.1.2 Absorption Time of a Resonant Photon 29
4.1.3 Lifetime of an Excited State 29
4.1.4 Time for Excitation/Decay Cycle 29
4.1.5 Probability of Returning to Original Ground State . 30
4.1.6 Probability of Reaching the LCR 30
4.2 Modification of the Racah Intensities 30
4.3 Summary 31

4.3.1 Previous Method: Monte-Carlo Type Simulation . . 31
4.4 Interaction Loop 32
4.4.1 Preliminary Steps 33
4.4.2 Interaction Loop 34
4.4.3 Simulation of Complete Run 36

5 Results 39

5.1 Initial Test 39
5.2 Temperature, CEC-LCR Distance and Power 40
5.2.1 Temperature 40
5.2.2 CEC-LCR Distance 41
5.2.3 Laser Power 42

6 Conclusion 49

Appendices 50

A Written Code 51

LIST OF TABLES

Table page

5–1 Parameters required for the simulation of a hyperfine spectrum. 40

LIST OF FIGURES

Figure		page
2–1	The location of the CFBS experiment	5
2–2	Schematic of the CFBS experiment at TRIUMF	6
2–3	The charge exchange cell.	8
2–4	Schematic of the light collection region.	8
3–1	Hyperfine spectrum and level-scheme for Gallium-69.	10
3–2	Oblate vs. Prolate vs. Spherical	14
4–1	Demonstration of the effects of optical pumping on the relative peak heights for a hyperfine spectrum of Francium-208.	26
4–2	Toy model of a hyperfine system with two ground states.	27
4–3	Flow chart detailing the steps undertaken by the alternative algorithm to follow the atom as it moves through the IR.	32
5–1	Comparison between a measured spectrum of Gallium-69 and a spectrum simulated.	39
5–2	Reduced χ^2 statistic as a function of the temperature used in the simulation of a Gallium-69 hyperfine spectrum.	41
5–3	The effects of the temperature on the hyperfine spectrum of Gallium-69.	42
5–4	The effects of changing the CEC-LCR distance on a simulated spectrum of Gallium-69.	43
5–5	The effects of the power of the exciting laser on a simulated Gallium-69 spectrum for powers between 0.1 and 40 mW.	43
5–6	The effects of the power of the exciting laser on a simulated Gallium-69 spectrum for powers between 50 and 100 mW.	44
5–7	Level-scheme of Rubidium-87.	45
5–8	Comparison between the simulated and measured hyperfine spectra of Rubidium-87 for different laser powers.	46

5–9 Continuation of Fig. 5–8. 47

5–10 The final set of spectra exploring the effect of the laser power on the hyperfine spectrum on Rubidium-87. 48

CHAPTER 1
Introduction

First observed in 1892 [1], the splitting of the spectral line of a single atomic transition, now known as the hyperfine splitting or structure of a transition, was theoretically described in 1924 by Wolfgang Pauli[2]. The development of quantum mechanics allowed Pauli to propose that the hyperfine splitting of a transition arose from the interaction of the orbital electrons and a small nuclear magnetic moment. In 1931, H. Schüler and T. Schmidt proposed the additional contribution of a nuclear electric quadrupole moment to the hyperfine splitting, completing the modern understanding of the interaction mechanisms[3].

The existence of hyperfine structure offers the unique opportunity to study the structure of the nucleus of an atom by probing the structure of a particular electronic transition. The nuclear magnetic moment proposed by Pauli depends on the spin of the nucleus, while the electric quadrupole moment described by Schüler and Schmidt depends on the distribution of charge in the nucleus. If the nuclear spin and the angular momentum state of the electron in both the ground and excited states are known, then the expected hyperfine structure can be determined by up to four parameters. Known as the hyperfine coefficients, these parameters describe the strength of the electron-nucleus interactions that give rise to the hyperfine structure. If the hyperfine spectrum of a transition can be measured empirically, the hyperfine coefficients and, by consequence, the nuclear structure can be determined.

Laser spectroscopy is a technique through which the hyperfine spectrum of a transition can be measured. Briefly, atoms (or ions) are exposed to laser

radiation. The frequency of this radiation is scanned such that, in the rest frame of the atom/ion, it comes into resonance with an allowed atomic transition. For reasons of efficiency when working with radioactive beams, the collinear geometry is used. The laser frequency is scanned by Doppler shifting the atoms/ions into resonance, rather than changing the frequency of the laser itself. Through the adjustment of their velocity, the atoms/ions can be moved in to and out of resonance with a chosen transition. Resonant velocities (and thus energies) will excite electrons through a hyperfine transition. The subsequent de-excitation of these electrons produces an excess of photons that can be measured using a set of light collection instruments. The location of these peaks with respect to each other determine the values of the hyperfine parameters and, in turn, the nuclear structure.

As with all experimental techniques, laser spectroscopy has its drawbacks. Among others, an effect known as optical pumping can severely change the outcome of a measurement. Optical pumping occurs when the atoms are exposed to the laser for a significant time before passing through the light collection region. This prolonged exposure to the laser can change the ground state distribution of the atoms, which in turn can cause certain hyperfine peaks to be drowned out or emphasized, altering the results of the ensuing hyperfine coefficient calculations. The strength of optical pumping depends on the isotope being investigated, the power of the exciting laser as well as the overall geometry of the experimental set up.

This work develops a procedure through which the effects of optical pumping on a given hyperfine spectrum can be simulated. In particular, this work focuses on the laser spectroscopy experiment set up at TRIUMF, Canada's national nuclear physics laboratory. The following Chapter briefly outlines TRIUMF's general structure, as well as how laser spectroscopy is done on

site. Chapter 3 provides a theoretical background to the mechanisms that lead to hyperfine splitting, while chapter 4 describes and demonstrates the effects of optical pumping on a hyperfine spectrum. The methods used to simulate the effects of optical pumping at TRIUMF are also presented in this section, with the results presented in Chapter 5. A summary and some concluding remarks are given in Chapter 6, and, finally, the developed program is found in the appendix.

CHAPTER 2
Laser Spectroscopy at TRIUMF

This chapter is intended as a brief introduction to the laser spectroscopy experiment present at TRIUMF, with special emphasis on the parts relevant to this work. A more complete description of the experiment can be found in [4].

As stated in the previous chapter, collinear laser spectroscopy operates by bringing a particle beam into resonance, through Doppler tuning, with a co-propagating (or counter-propagating, as is the case at TRIUMF) laser, which excites transitions in the electronic structure of the particles. The photons that are produced as a result of the de-excitation are then measured by light collection instruments. Located in the ISAC I (Isotope Separator and ACcelerator) experimental hall at TRIUMF, as shown in Fig. 2–1, the Laser Spectroscopy experiment at TRIUMF, more specifically known as the Collinear Fast-Beam laser Spectroscopy (CFBS) experiment, is shown in Fig. 2–2.

At TRIUMF, radioactive atoms are produced by 500 MeV protons impinging on a heavy target, inducing spallation. The products of the spallation then diffuse out of the target material, effuse from the target to the ion source, where they are ionized, accelerated and mass separated using a mass separator with resolution $m/\Delta m \approx 2000$, where m is the mass of the atom. [4] After the required atoms have been selected, they are then directed to the CFBS experiment, detailed below. In general, the CFBS group studies very exotic ions, i.e. ions that have low production rates.

2.1 Radio Frequency Quadrupole (RFQ) Trap

The ions enter the CFBS experiment as a continuous beam, where they first encounter a radio frequency quadrupole (RFQ) Paul Trap [4]. Here, the

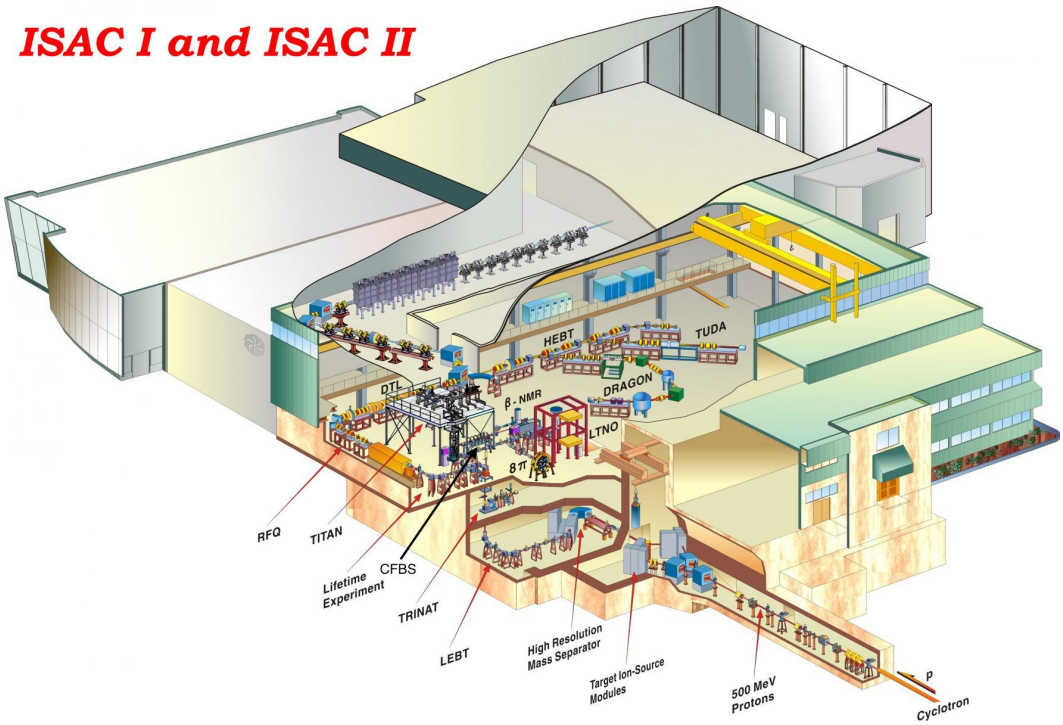

Figure 2–1: The location of the CFBS experiment within the ISAC I experimental hall, as well as the locations of the beamline and other experiments present at TRIUMF.

atoms can enter the RFQ trap and are collected for a pre-determined collection time, after which they are released in bunches. Bunching the atoms helps to significantly reduce background counts. Briefly, the light collection system is triggered on the release of the ion bunches, reducing the available time for background photons to be counted. As the light collection system is only sensitive to photons for the time window during which the ion bunch passes through the interaction region, background counts are also only collected for this time. Alternatively, photons are collected continuously, whether or not there are ions in the interaction region, allowing the signal to noise ratio to diminish over time. Ideally, the two methods produce the same signal, but with the latter have a significantly higher background. In general, the background is formed by dark counts from the photo-multiplier and actual photons scattered around the vacuum system. When continuously collected, the background is

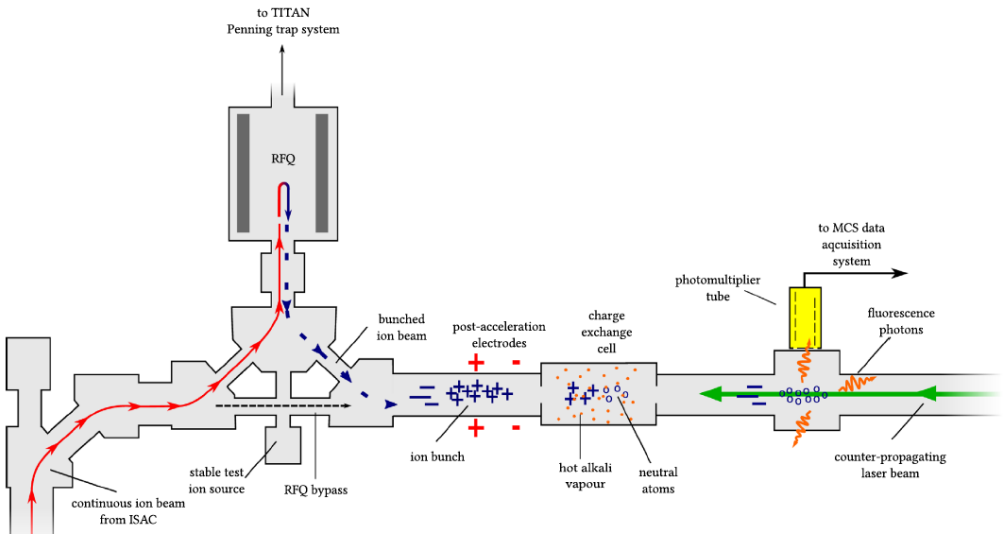

Figure 2–2: Schematic of the CFBS experiment at TRIUMF.[4] Radioactive ions produced in the target area are accelerated towards the experiment.

the rate of these events multiplied by the collection time. When the beam is pulsed, the background is the rate of the background events times the pulse length times the number of pulses per second. A typical pulse length is roughly $10\mu s$ at about 100 pulses per second [4].

2.2 Charge Exchange Cell (CEC)

If the aim is to investigate transitions in a neutral atom, then the ions must regain their lost electron. This is the role of the charge exchange cell (CEC), shown in detail in Fig. 2–3. Using an alkali-metal vapour that is circulated perpendicularly to the direction of the beam, the CEC provides a source of electrons for the oncoming ions to capture. This introduces an issue, however. As the alkali-metal vapour can not be entirely contained to the CEC, any light collection instruments, such as a photo-multiplier tube, must be located further down the beamline. This is done to avoid the growth of an alkali-metal coating on the light-collection surfaces which would significantly hamper the collection of resonant photons as the experiment progresses. This

decision provides the *raison d'être* for this work, as it introduces the opportunity for optical pumping, discussed in detail in Chapter 4. Since the ions are neutralized in the CEC, they can no longer be accelerated through the use of an electrostatic potential. As such, they must be brought into resonance before they enter the interaction region. This is done using a set of electrodes present in front of the CEC, shown in Fig. 2–2, as well as floating the CEC.

In the case of transitions present in the ion, then the CEC is unneeded, and the final acceleration is done using a mesh present within the LCR, detailed in the next section. The location of the mesh is chosen such that the ions are in resonance just as they pass the light collection system, removing the possibility that optical pumping could significantly affect the results of the experiment.

2.3 Light Collection Region (LCR)

Located roughly 40 cm down the beamline from the CEC, the light collection region (LCR) (Fig. 2–4) houses the equipment necessary for detecting the photons emitted when a beam of ions/atoms is in resonance with a counter propagating laser. A concave mirror located opposite the photo-multiplier tube (PMT) allows all photons within the 5% solid angle of the detection system to be collected by a series of light collection optics, placed in front of the PMT, designed to optimize photon detection efficiency at a particular wavelength. Using knowledge of the laser frequency, the beam energy and photon counts, the energies of the hyperfine transitions can be determined.

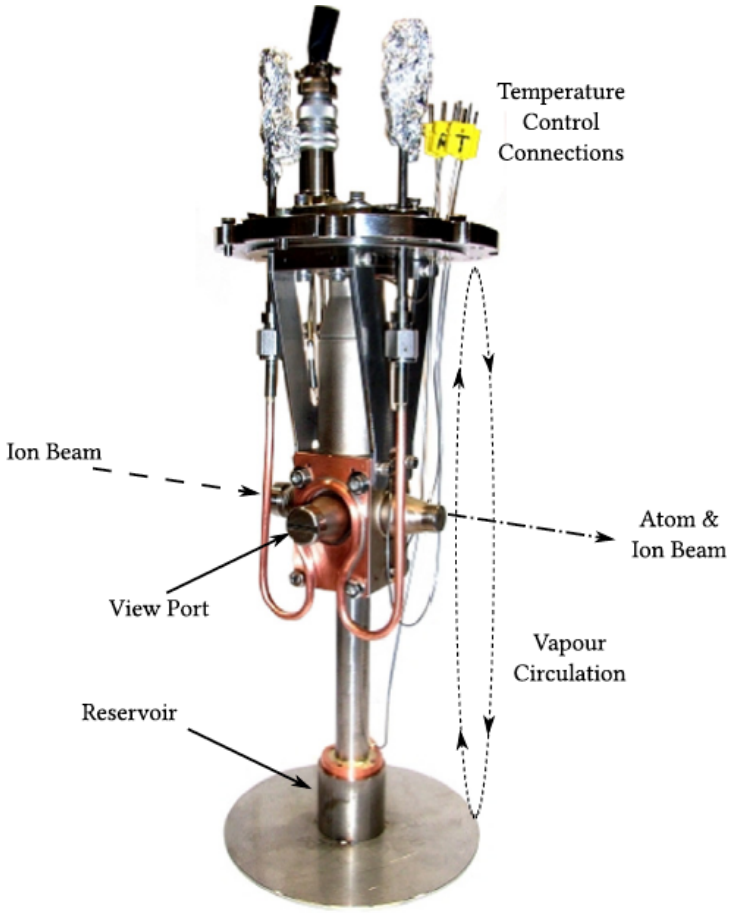

Figure 2–3: The charge exchange cell allows oncoming ions to be neutralized through collision with a perpendicularly flowing alkali-metal vapour.[4]

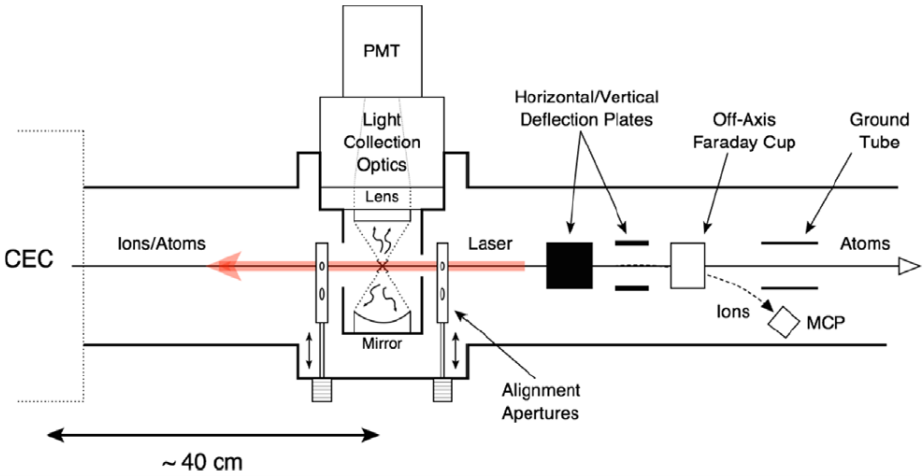

Figure 2–4: Schematic of the light collection region. Photons emitted through atom/laser interactions are directed towards a photo-multiplier tube using a combination of mirrors and lenses [4].

CHAPTER 3
Theory of Laser Spectroscopy

In this chapter, the theoretical background necessary to the understanding and simulation of a hyperfine spectrum is presented. § 3.1 describes how the features of a hyperfine spectrum are linked to physical properties of a nucleus, while § 3.2 outlines the way in which lasers interact with atoms. Note: Throughout this section, a variable written in a bold typeface is vector valued, while its non-bold counterpart is its magnitude.

3.1 Anatomy of a Hyperfine Spectrum

How can the properties of a hyperfine spectrum, such as that of ^{69}Ga shown in Fig.3–1, be translated into measurements of the physical properties of the nucleus? The hyperfine spectrum is, after all, the result of probing the electronic structure of the atom. The answer is that the electrons interact with the nucleus through several mechanisms, each of which will be described in this section. To begin, however, consider the following system: An electron transitions from a ground state $|g\rangle$ to an excited state $|e\rangle$. More precisely $|g\rangle$ and $|e\rangle$ are defined as

$$|g\rangle = |n_g, \mathbf{J_g}, \mathbf{J_{g,z}}\rangle \tag{3.1}$$

$$|e\rangle = |n_e, \mathbf{J_e}, \mathbf{J_{e,z}}\rangle, \tag{3.2}$$

where $n_{g,e}$ are principal quantum numbers, and $\mathbf{J_{g,e}} = \mathbf{L_{g,e}} + \mathbf{S}$ and $\mathrm{J}^z_{g,e}$ are the angular momentum and projection of the angular momentum on an axis of quantization z, respectively. $\mathbf{L}$ is the orbital angular momentum and $\mathbf{S}$ the

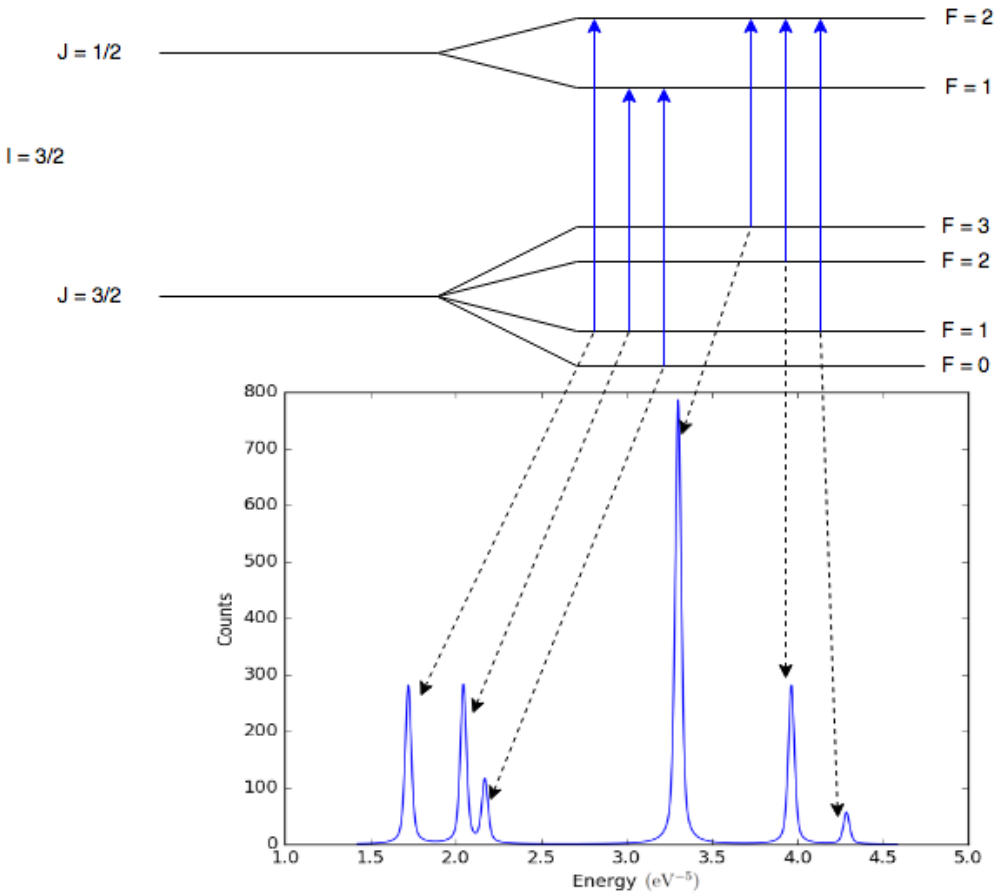

Figure 3–1: Hyperfine spectrum and level-scheme for the $4P_{3/2} \rightarrow 5S_{1/2}$ transition in atomic Gallium-69. Photon counts are shown on the vertical axis, while the horizontal shows the energies of the photons. Each allowed transition in the level-scheme is linked to the relevant peak in the hyperfine spectrum.

spin of the electron. Next, if nucleus of the atom in which this transition is occurring has angular momentum $\mathbf{I}$, then a new vector, $\mathbf{F}$, can be defined as

$$\mathbf{F_{g,e}} = \mathbf{I} + \mathbf{J_{g,e}} \tag{3.3}$$

$\mathbf{F}$ describes the total angular momentum state of the atom, so $|g\rangle$ and $|e\rangle$ can be rewritten as

$$|g\rangle = |n_g, \mathrm{F_g}, \mathrm{F_{g,z}}\rangle \tag{3.4}$$

$$|e\rangle = |n_e, \mathrm{F_e}, \mathrm{F_{e,z}}\rangle \tag{3.5}$$

For a fixed I, F can range from $(|\mathrm{I} - \mathrm{J}|)$ to $(|\mathrm{I} + \mathrm{J}|)$.

3.1.1 Peak Energies

The energy of the electrons depends on the various electron-nucleus interactions present in the atom. For the purposes of this work, only three interactions aer considered. These are the isotope, magnetic dipole and electric quadrupole shifts, which lead to energy shifts on the order of roughly $10^{-7} - 10^{-4}$ eV [5]. There are higher order interactions (magnetic octopole, electric hexadecapole), however their effects are far below the resolution of $\approx 10^{-8}$ eV of the experimental set-up employed at TRIUMF[6].

Isotope Shift

The isotope shift is measured with respect to a reference isotope. As neutrons are added or removed from a nucleus, the charge distribution, as well as the mass, of the nucleus changes. This leads to three different effects on the energies of the electrons.

The change in the mass of the nucleus leads to what is known as the Mass Shift, ΔE_M. The Mass Shift between two isotopes with mass numbers A and A' is given by [7]

$$\Delta E_M = \frac{m_{\mathrm{A}} - m_{\mathrm{A}'}}{2 m_{\mathrm{A}} m_{\mathrm{A}'}} \left(\sum_i \mathbf{p}_i + 2 \sum_{i>j} \mathbf{p}_i \cdot \mathbf{p}_j \right) \tag{3.6}$$

where m_{A} and $m_{\mathrm{A}'}$ are the isotope masses, and $\mathbf{p}_i$ is the momentum of the i^{th} election. The first term is the Bohr reduced mass equation arising from the change in the center of mass of the system.

The change in the charge distribution of the nucleus produces the Field Shift. While the typical nucleus is far smaller the wavefunction of a typical orbital electron, the effect is still important. The energy of a nucleus in the charge density produced by the electrons at the origin, E_F, is given by

$$E_F = \frac{Ze^2}{6\epsilon_0}|\psi(0)|^2 \left\langle r_{ch}^2 \right\rangle \tag{3.7}$$

where ϵ_0 is the permitivity of free space, Z is the proton number, e is the fundamental charge, $\psi(0)$ is the value of the electron wavefunction at the nucleus. $\left\langle r_{ch}^2 \right\rangle$ is the mean-square charge radius of the nucleus, defined as

$$\left\langle r_{ch}^2 \right\rangle = \frac{\int_0^\infty \rho(\mathbf{r}) r^2 dV}{\int_0^\infty \rho(\mathbf{r}) dV} \tag{3.8}$$

The field shift between two isotopes is then given by

$$\Delta E_F = \frac{Ze^2}{6\epsilon_0}\Delta|\psi(0)|^2 \Delta \left\langle r_{ch}^2 \right\rangle \tag{3.9}$$

In total, then, the isotope shift $\Delta E_{\mathrm{A,A'}}$ is given by

$$\Delta E_{\mathrm{A,A'}} = \Delta E_M + \Delta E_F \tag{3.10}$$

Typically, ΔE_M can be calculated beforehand. ΔE_F, however, must be determined experimentally, due to the difficulties associated with calculating $\Delta|\psi(0)|^2$.

Magnetic Dipole Interaction

A nucleus with a non-zero nuclear spin $\mathbf{I}$ will have a magnetic dipole moment, given by

$$\boldsymbol{\mu}_\mathbf{I} = g_\mathrm{I}\mu_\mathrm{N}\mathbf{I} \tag{3.11}$$

where g_I is the g-factor and μ_N is the nuclear magneton.[8] The interaction of μ_I with the magnetic field produced by the electrons, $\mathbf{B_e}$, creates a shift in

the energy of the orbiting electrons. Provided the electrons occupy an angular momentum state $\mathbf{J} \neq 0$ (since $\mathbf{J} = 0 \rightarrow \mathbf{B_e} = 0$), the Hamiltonian for this interaction is given by

$$\mathcal{H} = -\boldsymbol{\mu}_\mathbf{I} \cdot \mathbf{B_e} \tag{3.12}$$

This interaction leads to a shift, ΔE_{μ_I}, in the energy of the atomic states by

$$\Delta E_{\mu_I} = \frac{AK}{2} \tag{3.13}$$

where $K = \mathrm{F(F+1) - I(I+1) - J(J+1)}$ and

$$A = \frac{\mu_\mathrm{I} \mathrm{B_e}}{\mathrm{IJ}} \tag{3.14}$$

Electric Quadrupole Interaction

The electric quadrupole moment is used to describe the distribution of charge in a nucleus. For a nucleus composed of n protons and $\mathbf{I} \geqslant 1$, the electric quadrupole moment, Q, is given by

$$\mathrm{Q} = \sum_i^n (3z_i^2 - r_i^2) \tag{3.15}$$

where $r_i^2 = x_i^2 + y_i^2 + z_i^2$ for a chosen z-axis. Noting that the deformations described by Q are defined with respect to the $z-$axis, Fig. 3–2 shows how different values of Q translate into physical differences in the charge distribution of the nucleus. If $\mathrm{Q} < 0$, then the nucleus is stretched in the $x - y$ plane (oblate). If $\mathrm{Q} > 0$, then the nucleus is stretched along the $z-$axis (prolate). $\mathrm{Q} = 0$ indicates that the nucleus is spherical.

In reality, direct measurement of Q is not feasible, as the nucleus is rotating. Instead, the spectroscopic quadrupole, Q_s, is measured. Q_s is defined as the projection of Q onto the axis of quantization of the nucleus, and is given

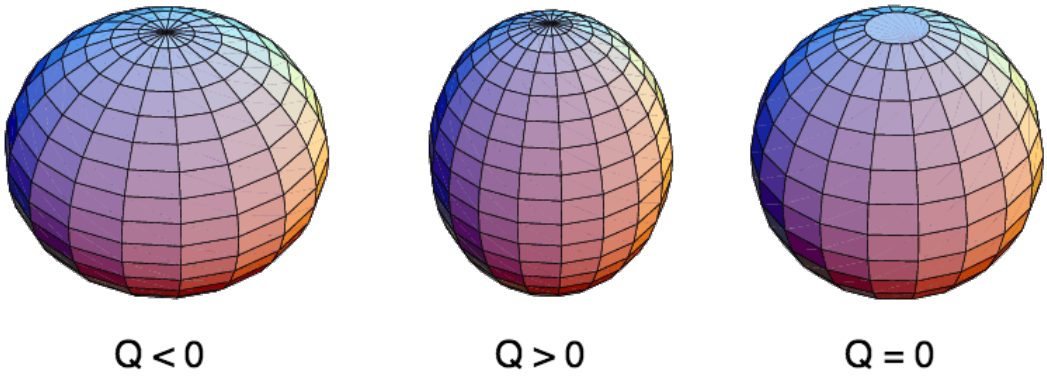

Figure 3–2: Shape of the nucleus for Q = 0 (spherical), Q < 0 (oblate) and Q > 0 (prolate).[9]

by

$$\mathrm{Q}_s = \frac{\mathrm{I}(2\mathrm{I}-1)}{(\mathrm{I}+1)(2\mathrm{I}+3)}\mathrm{Q}, \tag{3.16}$$

The use of Q_s as a measure of Q is valid under the assumption that the nuclear deformation is axially symmetric. Additionally, it is assumed that the axis of symmetry has a well defined direction with respect to **I**.

The Hamiltonian for the interaction between the spectroscopic electric quadrupole moment and the electric field produced by the electrons at the nucleus, E_N, is given by

$$\mathcal{H} = -\frac{1}{6}e\mathrm{Q}_s\nabla E_N \tag{3.17}$$

where

$$\nabla E_N = \frac{\partial^2 V}{\partial x_i \partial x_j}, \{x_j, x_k\} \in \{x, y, z\} \otimes \{x, y, z\}, \tag{3.18}$$

e is the fundamental charge and V is the electric potential. Recalling that the nuclear deformation is symmetric about the axis of quantization, the shift in energy is then given by

$$\Delta E_{\mathrm{Q_s}} = \frac{B}{4}\left[\frac{\frac{3}{2}K(K+1) - 2\mathrm{I}(\mathrm{I}+1)\mathrm{J}(\mathrm{J}+1)}{\mathrm{I}(2\mathrm{I}-1)\mathrm{J}(2\mathrm{J}-1)}\right] \tag{3.19}$$

where B is a hyperfine coefficient and is given by

$$B = e\mathrm{Q_s}\left\langle \frac{\partial^2 V}{\partial z^2} \right\rangle \tag{3.20}$$

Eq. 3.19 has singularities at I = $\frac{1}{2}$ and J=$\frac{1}{2}$. This captures the fact that in either case there is no coupling between the nucleus and the electric field gradient produced by the electrons, as an orbital angular momentum state of $\frac{1}{2}$ is isotropically distributed in space .

The Hyperfine Equation

The resonant energy of a transition between $|g\rangle = |n_g, \mathbf{F}_\mathrm{g} = \mathbf{I} + \mathbf{J}_\mathrm{g}\rangle$ and $|e\rangle = |n_e, \mathbf{F}_\mathrm{e} = \mathbf{I} + \mathbf{J}_\mathrm{e}\rangle$ is then given by

$$E_{hfs} = E_{fs} + \Delta E_{\mathrm{A,A'}} + \Delta E_{\mu_I}\Big|_{\mathrm{F_g},I,J_g}^{\mathrm{F_e},I,J_e} + \Delta E_{\mathrm{Q_s}}\Big|_{\mathrm{F_g},I,J_g}^{\mathrm{F_e},I,J_e}. \tag{3.21}$$

When a hyperfine spectrum is fitted, the fit parameters which govern the locations of the peaks are the hyperfine parameters A and B for both $|e\rangle$ and $|g\rangle$, as well as what is known as the centroid, ν_0. The centroid combines the fine structure energy and the isotope shift into one quantity. It is important to note that while the values of hyperfine coefficients can be directly linked to the physical properties of the nucleus, only the change in the centroid with respect to a reference isotope can be used to measure the change in the mean-square charge radius.

3.1.2 Peak intensities

The other notable characteristic of a hyperfine spectrum, the ratios of the peak intensities can give information as to the spin of the nucleus if the angular momentum states of the electron orbitals are known. The origin of the peak intensities is presented in more detail in the Angular Part of § 3.2, however in the interest of the completeness of this section, the result is presented here. The intensity of a transition from $|\mathrm{F_e}, \mathrm{J_e}, \mathrm{I}\rangle$ to $|\mathrm{F_g}, \mathrm{J_g}, \mathrm{I}\rangle$, relative to other

available transitions, is known as the Racah intensity and is given by

$$Intensity = (2F_e + 1)(2F_g + 1) \begin{Bmatrix} \mathrm{F_g} & \mathrm{F_e} & 1 \\ \mathrm{J_e} & \mathrm{J_g} & \mathrm{I} \end{Bmatrix}^2 \tag{3.22}$$

where the quantity in curly brackets is the Wigner 6-j symbol[7]. An important property of the Racah intensities is the dependence on I. In cases where the value of I may be ambiguous, the relative intensities of the transitions can be used to discriminate between values of I.

3.1.3 Peak Widths

The lineshape of the peaks is the result of three physical processes, outlined in this section. These three processes are of varying importance, depending on the properties of the atoms being probed, contributing Lorentzian or Gaussian profiles to the peak shape.

Natural Linewidth

The first addition to the linewidth of an atomic transition is the natural linewidth. The energy-time version of the uncertainty principal, $\Delta E \Delta t = \hbar$ leads to

$$\Delta\nu = \frac{\Delta E}{h} = \frac{1}{2\pi\tau_0} \tag{3.23}$$

where τ_0 is the mean lifetime of the state and $\Delta\nu$ is the full width half maximum of the Lorentzian profile describing the natural lineshape of an atomic transition[7].

Power Broadening

Stimulated emission occurs when an atom in an excited state is in the presence of photons with energy similar to an available atomic transition. In the case of laser spectroscopy, the laser provides the source of stimulating photons. Stimulated emission leads to power broadening, which depends on

the power of the laser. The lifetime of a state will decrease according to

$$\frac{1}{\tau} = \frac{1}{\tau_0}\sqrt{1 + \frac{I}{I_s}}, \tag{3.24}$$

where I is the laser intensity and I_s is the saturating laser intensity, which occurs when the rate of absorption is equal to the rate of stimulated emission on resonance. The expected lifetime of an excited electron decreases, resulting in a Lorentzian contribution to the lineshape as a consequence of the energy-time version of the uncertainty principal[7].

Doppler Broadening

Doppler broadening occurs when the atoms have a thermal velocity spread along the direction of propagation. This velocity spread leads to a shift in the frequency of the laser observed as by the atoms. The velocity distribution of a collection of atoms with mass m_A at temperature T, along an axis z, is given by the so-called Maxwell-Boltzmann distribution [10]

$$P(v_z) = \sqrt{\frac{m_A}{2\pi kT}} \exp\left(-\frac{m_A v_z^2}{2kT}\right) \tag{3.25}$$

where k is the Boltzmann constant and v_z is the velocity component of the atoms along the z-axis. The half width half maximum (HWHM) of this distribution is

$$\text{HWHM} = \sqrt{\frac{2\log(2)kT}{m_A}}. \tag{3.26}$$

For a Gaussian lineshape, the HWHM is also give by

$$\text{HWHM} = \sqrt{2\log(2)}\sigma_g \tag{3.27}$$

where σ_g the square root of the variance of the distribution, $\sigma_g^2 = kT/m_a$ in the case of a Gaussian profile. When an observer is moving relative to a source of radiation, the frequency of the radiation measured by the observer obeys

the following[11]

$$\nu_o = \nu_s \sqrt{\frac{1 + v/c}{1 - v/c}} \tag{3.28}$$

where ν_o and ν_s are the observed and source frequencies, respectively, v is the velocity of the observer relative to the source and c is the speed of light in a vacuum. Differentiating the above with respect to v, and assuming $v \ll c$ leads to

$$\begin{aligned} \frac{d\nu_o}{dv} =& 2\frac{\nu_s}{c} \\ d\nu_o =& \nu_s \left(\frac{8kT \log(2)}{m_A c^2} \right)^{1/2} \end{aligned}$$

$d\nu_o$ is the HWHM of the Gaussian lineshape that Doppler broadening contributes to the overall lineshape of the transition[7].

Voigt Profile

As the strengths of the above processes can change depending on the parameters of the experiment, a Voigt profile is used when fitting the hyperfine spectra. The Voigt profile, defined as a convolution of the Lorentzian and Gaussian profiles, has no exact analytic solution. For the purposes of this work, the Pseudo-Voigt profile, given below, is used.

$$\mathcal{V}(x) = \frac{1 - \epsilon}{\sigma_g \sqrt{2\pi}} \exp\left(\frac{(x - x_0)^2}{2\sigma_g^2} \right) + \frac{\epsilon \sigma}{\pi((x - x_0)^2 + \sigma^2)} \tag{3.29}$$

This is the weighted sum of a Gaussian and a Lorentzian where ϵ is a parameter that determines the relative contribution of the each and x_0 is the centroid. σ is the Voigt linewidth and $\sigma_g = \sigma/\sqrt{2\log 2}$ is defined such that the full width half maximum of the profile as well as its components is 2σ.[12]

3.2 Spontaneous Emission in Multi-Level Atoms

A hyperfine spectrum is constructed through the measurement of the photons emitted as electrons in excited states de-excite to lower energy states.

In order to simulate a hyperfine spectrum, then, it is necessary to understand the mechanisms through which electrons transition between energy levels in an atom.

Consider a two-level atom in an excited state. The wavefunction of the system is given by

$$|\psi\rangle = c_{e,0}e^{-i\omega_e t}\,|e,0\rangle + \sum_S c_{g,1}e^{-i(\omega_g+\omega)t}\,|g,1_S\rangle \tag{3.30}$$

where $S = (\boldsymbol{k}, \boldsymbol{\varepsilon})$ gives the wavevector $\boldsymbol{k}$ and polarization $\boldsymbol{\varepsilon}$ of an emitted photon, $\omega = kc$, ω_e and ω_g are the angular frequencies corresponding to the energy of the excited and ground states, respectively. [13] The time evolution of the two states is described by

$$i\frac{\mathrm{d}c_{e,0}(t)}{\mathrm{d}t} = \sum_S c_{g,1_S}(t)\Omega_S e^{-i(\omega-\omega_a)t} \tag{3.31}$$

$$i\frac{\mathrm{d}c_{g,1_S}(t)}{\mathrm{d}t} = c_{e,0}(t)\Omega_S^* e^{i(\omega-\omega_a)t} \tag{3.32}$$

where the coupling between each state is given by the Rabi frequency $\Omega_s = -\boldsymbol{\mu}\cdot\boldsymbol{E}_\omega/\hbar$. The electric dipole moment, $\boldsymbol{\mu}$ between two states is given by

$$\boldsymbol{\mu} = e\langle e|\,\boldsymbol{r}\,|g\rangle \tag{3.33}$$

and the electric field per mode is given by

$$\boldsymbol{E}_\omega = \sqrt{\frac{\hbar\omega}{2\epsilon_0 V}}\boldsymbol{\varepsilon}. \tag{3.34}$$

V is the volume over which the field is quantized and will eventually drop out. Integration of Eq. 3.32 and substitution of the result into Eq. 3.31, followed by further integration yields

$$\frac{dc_{e,0}(t)}{dt} = -\frac{\gamma}{2}c_{e,0}(t), \tag{3.35}$$

where

$$\gamma = \frac{\omega^3 \mu^2}{3\pi\epsilon_0 \hbar c^3} \tag{3.36}$$

is the decay rate for the population of the excited state, ω is the frequency of the transition and c is the speed of light in a vacuum. The mean lifetime of the excited state is given by $\tau = 1/\gamma$. For an excited state where multiple decay paths are available, the total decay rate, γ_t is given by

$$\frac{1}{\gamma_t} = \sum_i \frac{1}{\gamma_i} \tag{3.37}$$

where the γ_i are the partial decay rates for each decay path.

3.2.1 The Dipole Moment

In general, calculating the dipole moment $\mu = \langle e | \boldsymbol{\varepsilon} \cdot \boldsymbol{r} | g \rangle$ is not a simple task. In the simplest case (read hydrogenic wavefunctions), the Wigner-Eckart theorem states that the dipole moment can be split into two separate quantities in the following manner [13]

$$\mu_{eg} = e\mathcal{R}_{n_e J_e, n_g J_g} \mathcal{A}_{J_e J_e^z, J_g J_g^z} \tag{3.38}$$

where $\mathcal{R}_{n_e J_e, n_g J_g}$ and $\mathcal{A}_{J_e J_e^z, J_g J_g^z}$ are the radial and angular parts of the dipole moment, described in more detail below.

Radial Part

In most cases where the hyperfine structure is being probed, the radial part of the dipole moment only acts as an overall multiplicative factor for the strength of the coupling between the excited and ground states. This is due to the fact that all available ground states typically share the same radial wavefunction, likewise in the case of the excited states. The radial part is given by

$$\mathcal{R}_{n_e J_e, n_g J_g} = \langle R_{n_e J_e} | \boldsymbol{r} | R_{n_g J_g} \rangle = \int_0^\infty r^2 R_{n_e J_e}(r) r R_{n_g J_g}(r) dr \tag{3.39}$$

where the R_{nJ} are the hydrogenic radial wavefunctions of their respective states

$$R_{nJ}(r) = N_{nJ}\rho^J \exp(-\rho/2) J_{n-J-1}^{2J+1}(\rho) \tag{3.40}$$

where N_{nJ} is a normalization constant and $J_{n-J-1}^{2J+1}(\rho)$ are the Laguerre polynomials evaluated at $\rho = 2r/na_0$, where a_0 is the Bohr radius. The $J_{n-J-1}^{2J+1}(\rho)$ can be expanded in a power series

$$J_n^m(r) = \sum_{k=0}^{n} c_k r^k \tag{3.41}$$

It is possible to extend this analysis to atomic structures that have an isolated electron sitting outside a closed shell. This is done using the effective principal quantum number $n^* = n - \delta_J$, where δ_J is called the quantum defect and depends on the orbital angular momentum $\mathbf{J}$. This extended analysis is, however, not necessary, as an empirical measure of $\mathcal{R}^2_{n_e J_e, n_g J_g}$ is easily obtained, and remains constant over all hyperfine transitions. This is done through the use of the decay rate of the fine-structure transition, γ_f. From Eq. 3.37, the decay rate of the fine-structure excited state is given by

$$\frac{1}{\gamma_f} = 3\pi\epsilon_0\hbar c^3 \sum_i \frac{1}{\omega_i^3 \mu_i^2} \tag{3.42}$$

Substitution of Eq. 3.38 in to the above yields

$$\frac{1}{\gamma_f} = \frac{3\pi\epsilon_0\hbar c^3}{\mathcal{R}^2 e^2} \sum_i \frac{1}{\omega_i^3 \mathcal{A}_i^2} \tag{3.43}$$

where the subscripts on $\mathcal{R}$ and $\mathcal{A}$ have been dropped for convenience. Rearranging gives the following expression for $\mathcal{R}^2$

$$\mathcal{R}^2 = \frac{3\pi\epsilon_0\hbar c^3\gamma_f}{e^2} \sum_i \frac{1}{\omega_i^3 \mathcal{A}_i^2} \tag{3.44}$$

Note that this result allows $\mathcal{R}$ to take both negative and positive values. For the purposes of the calculations present in this work, however, only the square

of the radial part is important. As such, the degeneracy in Eq. 3.44 can safely be ignored.

Angular Part

Unlike the radial part of the dipole moment, the angular part changes depending on the F state of the excited and ground states. An outline of the procedure followed to find $\mathcal{A}$ is outlined in this section, a complete treatment of the calculation can be found in [13]

In the presence of hyperfine structure, the atomic eigenstates can be represented in the following manner

$$|n, F, F_z\rangle = \sum_i C_i \, |n, J, J_z\rangle \, |I, I_z\rangle \tag{3.45}$$

where $\mathbf{J} = \mathbf{J} + \mathbf{S}$, $\mathbf{S}$ is the spin of the electron and the C_i's are Clebsch-Gordan coefficients. The $\mathbf{J}$ states can further be decomposed into combinations of $\mathbf{J}$ and $\mathbf{S}$ states

$$|n, F, F_z\rangle = \sum_i C_i \, |I, I_z\rangle \sum_k C_k \, |n, J, J_z\rangle \, |S, S_z\rangle \tag{3.46}$$

This is possible since the optical electric field only couples the orbital angular momentum, $\mathbf{J}$, components of the eigenstates. The Clebsch-Gordan coefficients can be expressed as

$$C_i = \langle \mathrm{J}, \mathrm{J_z}; \mathrm{S}, \mathrm{S_z} | \mathrm{J}, \mathrm{J_z} \rangle = (-1)^{-\mathrm{J}+\mathrm{S}-\mathrm{J_z}} \sqrt{2\mathrm{J}+1} \begin{pmatrix} \mathrm{J}-\mathrm{S} & \mathrm{S} & \mathrm{J} \\ \mathrm{J}_z - \mathrm{S} & \mathrm{S}_z & -\mathrm{J}_z \end{pmatrix} \tag{3.47}$$

where the quantity in brackets is the Wigner 3-j symbol. Substituting Eq. 3.46 into the definition of μ gives

$$\begin{aligned}\mu = &\sum_{q=-1,0,1} e(-1)^{1+\mathrm{J_e}+\mathrm{J_g}+\mathrm{I}-\mathrm{F_{e,z}}}\mathcal{R}_{n_eJ_e,n_gJ_g} \\ &\times\sqrt{(2J_g+1)(2J_e+1)(2F_g+1)(2F_e+1)} \\ \times &\begin{Bmatrix} \mathrm{J}_e-\mathrm{S} & \mathrm{J}_e & \mathrm{S} \\ \mathrm{J}_g & \mathrm{L}_g-\mathrm{S} & 1 \end{Bmatrix} \begin{Bmatrix} \mathrm{J}_e & \mathrm{F}_e & \mathrm{I} \\ \mathrm{F} & \mathrm{J}_g & 1 \end{Bmatrix} \begin{pmatrix} \mathrm{F}_g & 1 & \mathrm{F}_e \\ \mathrm{F}_{g,z} & q & -\mathrm{F}_{e,z} \end{pmatrix}\end{aligned} \tag{3.48}$$

where the quantity in the curly brackets is not a 3-j symbol but a 6-j symbol, and q is the polarization of the electric field (1,0,-1). Recalling that $\mathcal{R}_{n_eJ_e,n_gJ_g}$ is a multiplying factor only and can be pulled out of the summation, then the angular part of μ (Eq. 3.38) is given by

$$\begin{aligned}\mathcal{A} = &\sum_{q=-1,0,1} e(-1)^{1+\mathrm{J_e}+\mathrm{J_g}+\mathrm{I}-\mathrm{F_{e,z}}} \times \sqrt{(2J_g+1)(2J_e+1)(2F_g+1)(2F_e+1)} \\ &\times \begin{Bmatrix} \mathrm{J}_e-\mathrm{S} & \mathrm{J}_e & \mathrm{S} \\ \mathrm{J}_g & \mathrm{J}_g-\mathrm{S} & 1 \end{Bmatrix} \begin{Bmatrix} \mathrm{J}_e & \mathrm{F}_e & \mathrm{I} \\ \mathrm{F} & \mathrm{J}_g & 1 \end{Bmatrix} \begin{pmatrix} \mathrm{F}_g & 1 & \mathrm{F}_e \\ \mathrm{F}_{g,z} & q & -\mathrm{F}_{e,z} \end{pmatrix}.\end{aligned} \tag{3.49}$$

3.2.2 Selection Rules

The coupling of the ground state and excited state through the optical electrical field places restrictions on the change in the angular momentum state of the atom. In the case of transitions between orbital angular momentum states present in hyperfine atomic structures, only transitions where $\Delta\mathbf{F} = \pm 1, 0$ are permitted. These selection rules reflect conservation of angular momentum. Photons have angular momentum $\hbar$. The angular momentum of the photon can either be parallel, anti-parallel or perpendicular to the axis of quantization, reflecting $\Delta\mathbf{F}= \pm 1, 0$ respectively. Additionally, the transition $\mathbf{F}' = 0 \rightarrow \mathbf{F} = 0$ is forbidden. This is because $\mathbf{F}$ is a result of the coupling

between **I** and **J**. **F**' = 0 implies that **I** = 0 = **J**'. The emission of a photon requires a change in angular momentum, which is impossible if **F** = 0 = **I** + **J**.

3.3 Photon Scattering Rates

The rate at which photons are absorbed by atoms is an important factor in the simulation of hyperfine spectra. For a two level system, where the population of the the excited state ρ_e and the ground state ρ_g obey the conservation rule $\rho_e + \rho_g = 1$, the total scattering rate from a laser field is given by

$$\gamma_p = \frac{s_0/2}{1 + s_0 + (2\delta/\gamma)^2} \tag{3.50}$$

where s_0 is the on resonance saturation parameter $s_0 = I_l/I_s$, δ is the detuning parameter and γ is the decay rate of the excited state. I_l is the intensity of the laser field and I_s is the saturation intensity defined as

$$I_s \equiv \frac{\pi hc}{3\lambda^3\tau} \tag{3.51}$$

where λ is the wavelength of emission of a resonant photon and $\tau = 1/\gamma$ is the lifetime of the excited state. The detuning parameter can be defined as

$$\delta = |f_l - f_{res}| \tag{3.52}$$

where f_l is the frequency of the laser and f_{res} is the resonant frequency of the transition[13]. Eq. 3.50 provides an easy evaluation of the expected time for an on-resonance photon to be absorbed, which will be needed in the next chapter.

CHAPTER 4
Simulation of Optical Pumping

As mentioned in the Chapter 2, the distance between the CEC and the LCR introduces the possibility of optical pumping, a process that changes the ground state distribution of the atoms as they travel the distance between the two regions. This change in ground state distribution is induced by the interaction of the atoms with the laser before they reach the LCR. In an atomic system that has not interacted with a laser, the ground state distribution of the hyperfine levels is statistical.[14] The likelihood of an electron occupying hyperfine level **F** is proportional to $2F + 1$. In a system with N hyperfine ground states, each with $\mathbf{F} = \mathbf{F}_n$, where n = 1,2,3,..N, the probability of an electron occupying, the i-th level is given by [14]

$$\mathrm{Prob(F}_i) = \frac{2F_i + 1}{\sum_{j=1}^{\mathrm{N}} 2F_j + 1}. \tag{4.1}$$

However, as the electron goes through a series of excitation/decay cycles, certain ground states will be selected over others, depending on selection rules as well as transition probabilities. Optical pumping manifests itself through the modification of the relative peak heights in a hyperfine spectrum, as shown in Fig. 4–1, where the peak heights of a hyperfine spectrum of Francium show the effects of optical pumping. The expected peak heights as calculated by the Racah intensities are shown in red, and are compared to the intensities measured with the laser continuously on (solid black) and those measured when the laser was pulsed (black outline). The pulsed intensities are similar to the expected intensities, while those measured with a continuous wave (cw) laser deviate significantly.

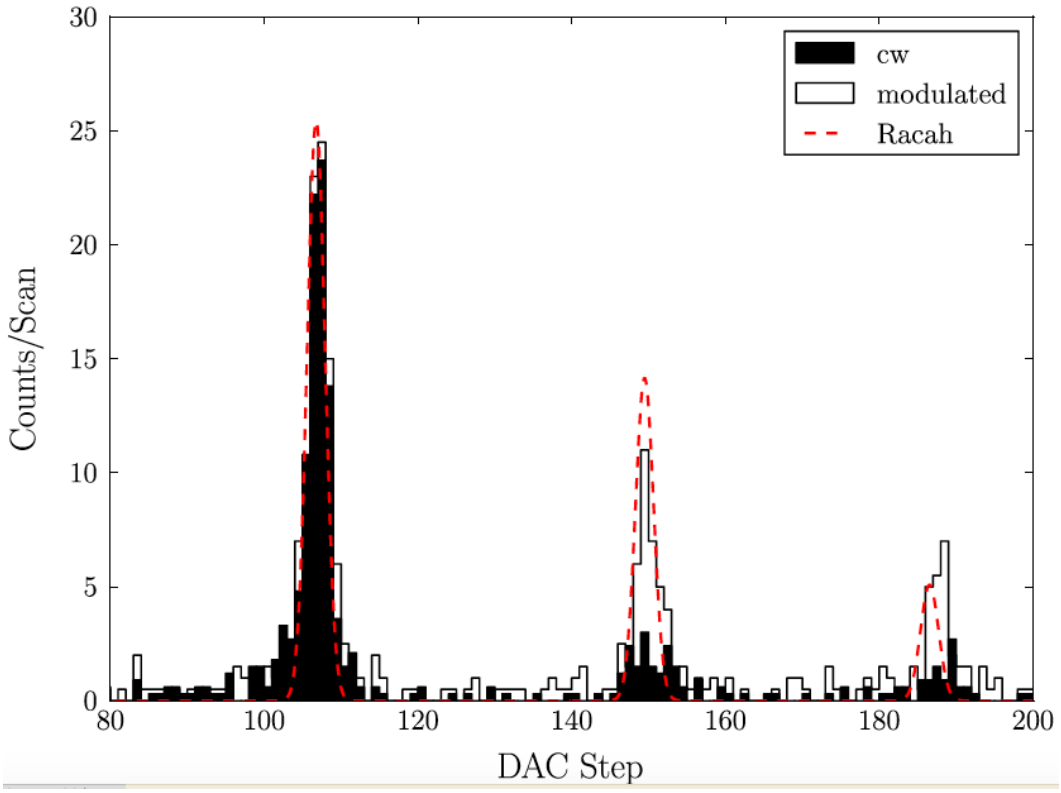

Figure 4–1: Demonstration of the effects of optical pumping on the relative peak heights for a hyperfine spectrum of Francium-208. The Racah intensities are shown in red, while the intensities measured for a continuous wave (cw) laser and a pulsed laser are shown in solid black and black lines, respectively. The Digital Analogue Converter (DAC) is proportional to the laser frequency. The cw measurements deviate significantly from the Racah intensities, while the pulsed measurements are closer to the expected intensities.[4]

To illustrate the effect of mechanisms of optical pumping, consider the following: A hyperfine system has two ground states, $\mathbf{F_1}$ and $\mathbf{F_2}$, as well as an excited state $\mathbf{F_3}$, as shown in Fig. 4–2. When the atom is in the excited state, it has probability $P(\mathbf{F_3} \rightarrow \mathbf{F_2})$ of decaying to the $\mathbf{F_2}$ state, and probability $1 - P(\mathbf{F_3} \rightarrow \mathbf{F_2})$ of decaying to the $\mathbf{F_1}$ state. If the atom is exposed to a laser resonant with the $\mathbf{F_2} \rightarrow \mathbf{F_3}$ transition, what is the probability that after time t the ground state of the atom is still $\mathbf{F_2}$? Say that the lifetime of the $\mathbf{F_2} \rightarrow \mathbf{F_3}$ transition is τ, and that the average time for a resonant photon to be absorbed is t_{abs}. Then the number of excitation/decay cycles in time t,

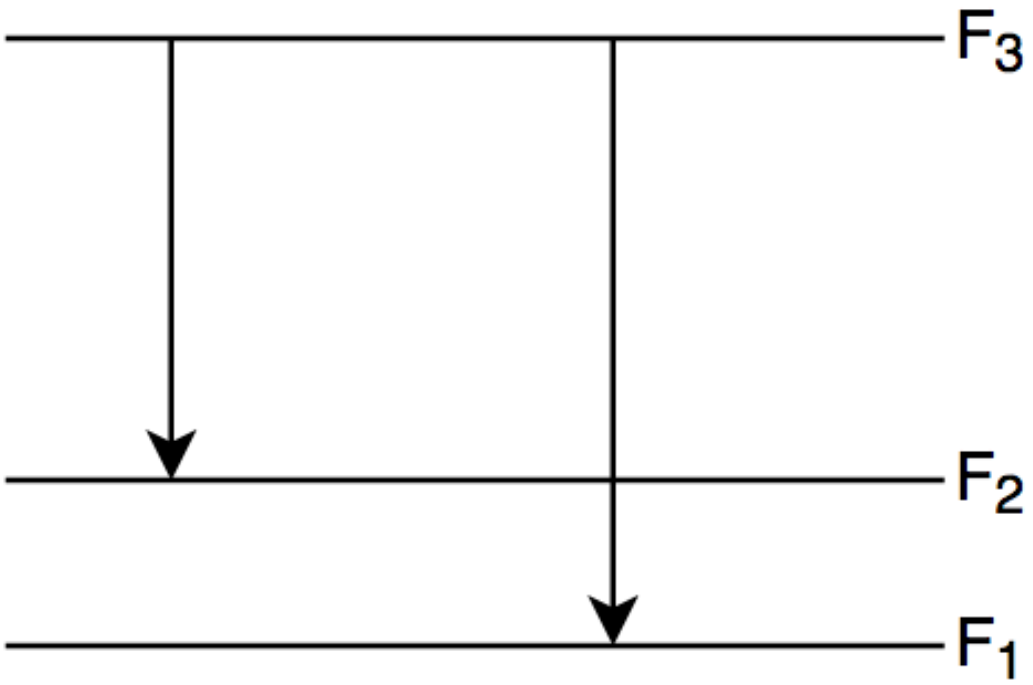

Figure 4–2: Toy model of a hyperfine system with two ground states, $\mathbf{F_1}$ and $\mathbf{F_2}$, and a single excited state $\mathbf{F_3}$. If this system is exposed to a laser resonant with the $\mathbf{F_2} \rightarrow \mathbf{F_3}$ transition, then as the atom goes through excitation and decay cycles, the chances of having an electron in $\mathbf{F_2}$ available for excitation decrease.

N_{cycles}, is

$$N_{\text{cycles}} = \frac{t}{\tau + t_{\text{abs}}}. \tag{4.2}$$

rounded down to the closest integer. If at any time, the atom decays to the $\mathbf{F_1}$ state, then it is no longer on resonance and the chances of a photon being absorbed are negligible. As such, the probability that the atom is in $\mathbf{F_2}$ after N_{cycles} is

$$P(\mathbf{F_2}) = \mathbf{P}(\mathbf{F_3} \rightarrow \mathbf{F_2})^{\mathbf{N}_{\text{cycles}}} \tag{4.3}$$

As $P(\mathbf{F_3} \rightarrow \mathbf{F_2}) < \mathbf{1}$, then the chances of finding an electron in the $\mathbf{F_2}$ state decrease as t increases. If, for example, one began measuring the number of resonant photons emitted after time t for a collection of atoms with the above hyperfine structure, the number of photons measured would be reduced by a factor of $P(\mathbf{F_2})$. This calculation is the basis for the method used in this work

to measure the effect of optical pumping on the atoms being investigated at the CFBS, presented in the following section.

4.1 Optical Pumping as a Modification to the Racah Intensities

To evaluate the effects of optical pumping on a hyperfine spectrum collected at the CFBS experiment, the toy model presented above need only be expanded on. The important quantities are the time an atom interacts with the laser before entering the LCR, the time it takes for a resonant photon to be absorbed, the lifetimes of each excited state and the probability of an electron decaying to the ground state from which it originated. The computation of each of these quantities is shown in this section, after which they are combined to calculate how the Racah intensity for each transition must be modified to show the effects of optical pumping.

4.1.1 Interaction Time

The interaction time, t_{int} is the time that the atom will be possibly be interacting with the laser before entering the LCR. Its calculation is straightforward. If the distance between the CEC and the LCR is d, and the atoms are moving at a velocity v, then the interaction time is

$$t_{\text{int}} = \frac{d}{v}. \tag{4.4}$$

While d is a static quantity, v changes depending on the frequency of the laser and the resonant frequency of the transition in question. As mentioned in Chapter 2, the CFBS fixes the frequency of the laser and uses electrodes to alter the speed of the oncoming atoms, shifting the frequency observed by the atoms. Knowing the initial energy of the beam E_b and the mass of the atoms m_a, the initial velocity of the atoms is

$$v_{\text{init}} = \sqrt{\frac{2E_b}{m_a}}, \tag{4.5}$$

If the resonant frequency of a transition is f_{res} and the frequency of the laser is f_{las}, then the velocity at which the atom will observe f_{res}, v_{res}, is described by [15]

$$f_{\text{res}} = f_{\text{las}}\sqrt{\frac{1 + v_{\text{res}}/c}{1 - v_{\text{res}}/c}}. \tag{4.6}$$

Rearranging yields the following expression for v_{res}

$$v_{\text{res}} = c\frac{(f_{\text{res}}/f_{\text{las}})^2 - 1}{(f_{\text{res}}/f_{\text{las}})^2 + 1} \tag{4.7}$$

and

$$t_{\text{int}} = \frac{d}{c}\frac{(f_{\text{res}}/f_{\text{las}})^2 + 1}{(f_{\text{res}}/f_{\text{las}})^2 - 1} \tag{4.8}$$

4.1.2 Absorption Time of a Resonant Photon

For a chosen transition, what is the expected time, t_{abs} that passes before a resonant photon is absorbed by the atom, given a laser field of intensity I? This is simply the inverse of the scattering rate, as described in Eq. 3.50, evaluated at resonance, i.e. $\delta = 0$

$$t_{\text{abs}} = \left(\frac{s_0\gamma/2}{1 + s_0}\right)^{-1}. \tag{4.9}$$

4.1.3 Lifetime of an Excited State

This quantity is already known. The inverse of Eq. 3.36 gives the lifetime, τ, of a particular transition

$$\tau = \frac{3\pi\epsilon_0\hbar c^3}{\omega^3\mu^2}. \tag{4.10}$$

4.1.4 Time for Excitation/Decay Cycle

Combining the results from the two above sections, the average time that it takes for an atom to go through an excitation/decay cycle, assuming that

it returns to the ground state that it was in before excitation, t_{cycle}, is

$$t_{\text{cycle}} = t_{\text{abs}} + \tau \tag{4.11}$$

$$= \left(\frac{s_0 \gamma / 2}{1 + s_0} \right)^{-1} + \frac{3\pi\epsilon_0 \hbar c^3}{\omega^3 \mu^2} \tag{4.12}$$

4.1.5 Probability of Returning to Original Ground State

The probability of an atom decaying to the ground state from which it was excited is computed by comparing the decay rates of all possible transitions that share the same excited state as the transition in question, i.e.,

$$P(\text{OGS}) = \frac{\gamma_{\text{OGS}}}{\sum_{\text{PT}} \gamma_{\text{PT}}} \tag{4.13}$$

where $P(\text{OGS})$ is the probability of the atom returning to the original ground state, γ_{OGS} is the decay rate of the transition that results in the return to the original ground state and γ_{PT} is the decay rate of all possible transitions that share the same excited state as the transition in question.

4.1.6 Probability of Reaching the LCR

Finally, the probability of an atom reaching the LCR without changing its ground state is given by

$$P(\text{OGS at LCR}) = \left(\frac{\gamma_{\text{OGS}}}{\sum_{\text{PT}} \gamma_{\text{PT}}} \right)^{\frac{t_{\text{int}}}{t_{\text{cycle}}}} \tag{4.14}$$

where $\frac{t_{\text{int}}}{t_{\text{cycle}}}$ is rounded down to the nearest integer, reflecting the fact the excitation/decay cycles are quantized events.

4.2 Modification of the Racah Intensities

Now that the probability of finding an atom in its original ground state when it reaches the LCR is known, the effects of optical pumping can be simulated through the modification of the Racah intensity for each transition.

For a given transition $\mathbf{F_e} \rightarrow \mathbf{F_g}$ the modified Racah intensity, $I_{R_{\text{mod}}}$, is

$$I_{R_{\text{mod}}} = P(\mathbf{F}_g \text{ at LCR})(2F_e+1)(2F_g+1) \begin{Bmatrix} F_g & F_e & 1 \\ J_e & J_g & \text{I} \end{Bmatrix}^2 \tag{4.15}$$

$$= \left(\frac{\gamma_{\text{OGS}}}{\sum_{\text{PT}} \gamma_{\text{PT}}} \right)^{\frac{t_{\text{int}}}{t_{\text{cycle}}}} (2F_e+1)(2F_g+1) \begin{Bmatrix} F_g & F_e & 1 \\ J_e & J_g & \text{I} \end{Bmatrix}^2 \tag{4.16}$$

which results from the combination of Equations 4.14 and 3.22.

4.3 Summary

In this Chapter, optical pumping was treated as a modification to the Racah intensities, which describe the intensities of hyperfine transitions. Optical pumping changes the ground state distribution of the atoms/ions before they enter the LCR. To simulate this effect, the probability of an atom reaching the LCR the without changing ground state was calculated (Sections 4.1.5 and 4.1.6) for each hyperfine transition. This probability was a function of the laser power, the distance between the CEC and the LCR, and the likelihood of the transition in question. Once the probability of an atom remaining in its original ground was known, the corresponding Racah intensity was multiplied to get the adjusted intensity for that particular transition.

4.3.1 Previous Method: Monte-Carlo Type Simulation

The method developed above is based on statistical ensembles describing the state of the atoms/ions as they pass through the experiment. Previously, a full simulation of each atom as it passed through the experiment was developed. This method was eventually abandoned due to the excessive computation time required. For posterity's sake, it is mentioned here.

In this section, the Monte-Carlo simulation of a hyperfine spectrum measured at TRIUMF is described in detail. §4.3.1 includes little more than a

graphical representation of the algorithm followed when the atoms are interacting with the laser. Each subsequent section is dedicated to an individual step in the algorithm, detailing the logic and computations required at that step. The final section of the chapter shows how a hyperfine spectrum is built through the repeated application of the interaction loop.

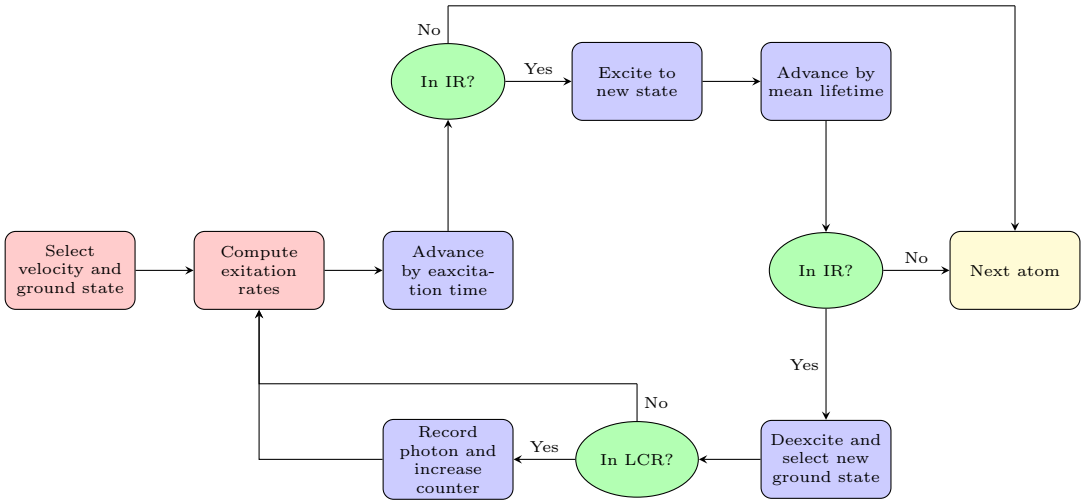

Figure 4–3: Flow chart detailing the steps undertaken by the algorithm to follow the atom as it moves through the IR. The green ellipses and blue rectangles compose the interaction loop of the simulation, where the atom interacts with the laser and goes through excitation/decay cycles. Finally, the yellow rectangle is the end point of the loop, and occurs when then atom has moved beyond the IR.

4.4 Interaction Loop

Fig. 4–3 shows each step taken an atom as it passes through the simulation. The red rounded rectangles represent preliminary steps in the simulation, where initial properties are imparted to the atom. The first preliminary step selects a velocity and ground state for the atom. The following step is the calculation of the likelihood of excitation for each allowed transition. This prepares the atom for what can be considered the main loop of the algorithm. Here, the atom and laser interact as the atom traverses the IR.

The interaction loop is composed of green ellipses and blue rectangles. Two of the three green ellipses represent regular checks to ensure that the

atom is still in the IR. If at any point the atom is found to have moved beyond the IR, then the algorithm moves on to the next atom. The third green ellipse is dedicated to checking if a photon released by the atom would be measured by the PMT. The evolution of the state and position of the atom is described by the blue rectangles.

4.4.1 Preliminary Steps

The first two steps select the initial properties given to the atom, determining how likely the atom is to interact with the laser. The two most important properties are the velocity and the ground state of the atom. Both are chosen through the sampling of their respective probability distributions.

Velocity Selection

The velocity of the atom v_a can be decomposed in to two elements: the mean velocity of the beam, v_m, and the thermal velocity v_T.

$$v_a = v_m + v_T \tag{4.17}$$

The mean velocity is determined by the energy of the beam and the mass of the atom, i.e.

$$v_m = \sqrt{\frac{2E_b}{m_A}} \tag{4.18}$$

where E_b is the energy of the beam and m_A is the mass of an atom with mass number A.

The thermal velocity is selected by sampling the Maxwell-Boltzmann distribution (Eq. 3.25). This is done using the Box-Muller transform, which samples a uniform distribution twice and converts the results into a sample of a normal distribution. A sample v_T, of a Maxwell-Boltzmann distribution

$$v_T = \sigma_{MB}\sqrt{-2\log x_1}\cos(2\pi x_2) \tag{4.19}$$

where $x_1, x_2 \in [0, 1]$ are two randomly generated numbers taken from a uniform distribution and σ_{MB} is the square root of the variance of the Maxwell-Boltzmann distribution.

Ground State Selection

For an atom with a coupled angular momentum state F_g as the ground state, the electron can occupy any of the $2F_g + 1$ projections on the axis of quantization. A particular projection, say $F_i \in [-F_g, -F_g + 1, ..., F_g - 1, F_g]$, has a probability of being occupied that is proportional to $2F_i + 1$. Taking the probability space occupied by each projection in to account, the probability that an electron occupies the projection F_i, $P(F_i)$, is given by

$$P(F_i) = \frac{2F_i + 1}{\sum_j 2F_j + 1} \tag{4.20}$$

Knowing this, the ground state can be chosen through the generation of a random number $x \in [0, 1]$ from a uniform distribution. Each projection is given a range of numbers from 0 to 1, proportional to Eq. 4.20. If x falls in the assigned range, then that ground state is chosen.

Computation of Excitation Rates

With the ground state and the velocity of the atom now selected, the probability that a transition will occur can be calculated. For each allowed transition between the chosen ground state F_g and an excited state $F_{e,i}$, the transition rate γ_i is given by Eq. 3.50. Note that the laser frequency f_l must be shifted according to Eq. 3.28.

4.4.2 Interaction Loop

The interaction loop of the algorithm is the place where the atoms undergo several instances of excitation and decay. Also included are regular checks to see in the atom would still be present in the in interaction region, as well as

whether or not a released photon would be measured by the light collection system present in the experiment.

Excitation Time

Once all the excitation rates have been computed, the atom can now be advanced by the expected time it takes for a transition to occur. This time is called the excitation time, t_e, and is given by

$$t_e = \sum_i \frac{1}{\gamma_i} \tag{4.21}$$

After time t_e, the atom is advanced a distance $d_e = t_e v_a$. If it is still in the interaction region, then an excited state F_e is chosen by sampling a uniform distribution where each transition is given a region proportional to $1/\gamma_i$, in similar style to the method used to select the ground state. If the atom is no longer in the interaction region after t_e, then it is discarded and the algorithm moves on to the next atom.

Advancing by the Mean Lifetime, Decay and Selection of New Ground State

Once the excited stated of the atom has been selected, then the atom is advanced a distance $d_l = t_l v_a$ where t_l is the mean lifetime of the excited state. The mean lifetimes of each excited state are computed (according to § 3.2) once at the beginning of the simulation, then stored for later use. If the atom is still in the interaction region after having moved d_l, then it decays into one of the allowed ground states. If not, then the simulation moves on to the next atom. As with the selection of the excited state, a uniform distribution is sampled, and each ground state $F_{g,i}$ is given a range of values proportional to the inverse of the lifetime of the transition from the excited state, F_e, to $F_{g,i}$.

Once a ground state is selected, a photon with energy given by Eq. 3.21 is "released". If the atom is in the light collection region, then this photon is recorded for later analysis. Additionally, a counter that keeps track of the number of photons collected at each beam energy is increased by one. If the atom is not in the LCR, then nothing is recorded, and the excitation-decay process begins again with the computation of excitation rates.

4.4.3 Simulation of Complete Run

In order to simulate a complete experimental run, a chosen number of atoms, say N, are passed in sequence through the above loop. This is done in turn for each beam energy in a list of energies that are selected such that the Doppler shifted laser energies range from the lowest energy to the highest energy transition, with some leeway on either side. This range can be called E_r. The graph of photon counts per beam energy is in fact the hyperfine spectrum. Alg. 1 shows the pseudo-code that is followed for the simulation of a collection of atoms passing through the experiment. Following Alg. 1 is a list of all the preliminary parameters needed by the simulation in order to compute the necessary quantities presented in this section.

Result: Simulation of complete hyperfine spectrum

Input all preliminary parameters;

for *Beam energy in* E_r **do**

  for *Each atom* **do**

    Run **interaction loop**;

    Record photon count;

  end

  Sum photon count into counts per beam energy;

end

Plot photon count at each beam energy;

Algorithm 1: Pseudo-code for the simulation of a complete hyperfine spectrum.

The preliminary parameters mentioned in the above pseudo-code refer to all the quantities required to perform a complete simulation of a hyperfine spectrum measured at TRIUMF. A list of these parameters is provided below, for completeness.

List of Preliminary Parameters and Their Symbols

- Isotope mass: m_A
- Ground J-state: $\mathbf{J_g}$
- Excited J-state: $\mathbf{J_e}$
- Nuclear spin: $\mathbf{I}$
- Principal quantum number of ground state: n_g
- Principal quantum number of excited state: n_e
- Magnetic dipole hyperfine coefficient of ground state: A_g
- Magnetic dipole hyperfine coefficient of excited state: A_e
- Electric quadrupole hyperfine coefficient of ground state: B_g
- Electric quadrupole hyperfine coefficient of excited state: B_e

- Beam temperature: T_b
- Laser frequency: f_l
- Laser intensity: I_l
- Fine structure transition energy: E_{fs}
- Number of atoms to simulate per beam energy: N_a
- Distance between CEC and LCR: d
- Length of LCR: d_{LCR}

CHAPTER 5
Results

This section presents and examines the results of the modeling outlined in the previous section. § 5.2 shows the effects of changing important input parameters, such as the temperature, on a simulated spectrum of Gallium-69.

5.1 Initial Test

As a first test, this Fig. 5–1 presents a comparison between a measured spectrum of Gallium-69 and a simulated spectrum generated using the parameters given in Table 5–1.

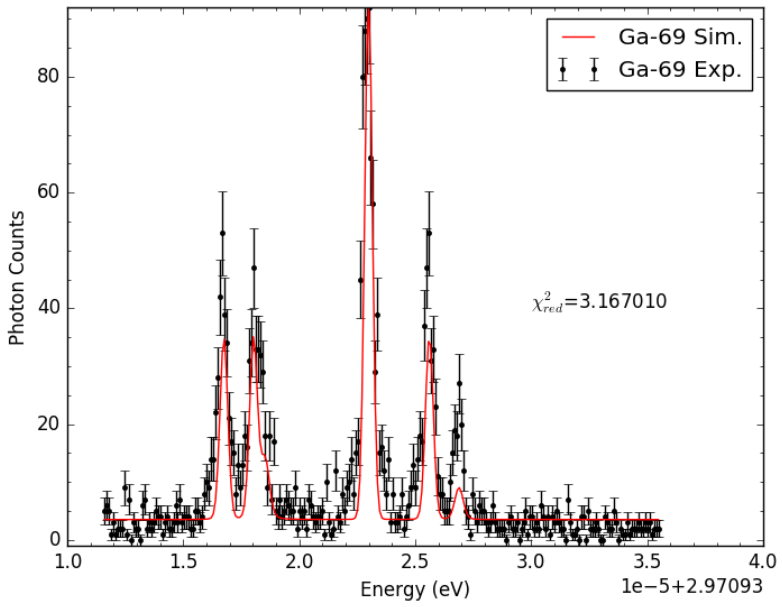

Figure 5–1: Comparison between a measured spectrum of Gallium-69 and a spectrum simulated using the parameters given in in Table 5–1.

A distinct difference in the peak widths between the simulated and measured spectra can be seen in Fig. 5–1, where the simulated spectrum has narrower peaks than the measured spectrum. A reduced χ^2 (defined as $\chi^2 =$

A_u (MHz)	A_l (MHz)	B_u (MHz)	B_l (MHz)
1070.908128	188.512676	0	68.333737

Temperature (K)	Power (mW)	CEC-LCR Dist. (m)
300	1.0	0.40

Table 5–1: Parameters required for the simulation of a hyperfine spectrum. The hyperfine parameters are from a previous measurement of the the spectrum of Gallium-69.[16] The power and CEC-LCR distance are measured quantities, while the temperature is estimated.

$\frac{1}{N}\sum_i^N \frac{(s_i-m_i)^2}{\sigma_i^2}$, where s_i is the simulated counts, and m_i and s_i are the measured counts and their uncertainty, respectively) statistic of 3.167010 is reported as a measure of accuracy between the simulation and data. Note that the second peak from the left is composed of two transitions. Since the temperature is merely an estimate based on the temperature of the intert gas used to cool the ions in the RFQ, it is possible that this estimation is inaccurate. Fig. 5–2 shows the reduced χ^2 statistic as a function of the temperature used in the simulation. The estimated temperature of 300 K is lower than the temperature that produces the lowest reduced χ^2 value, occurring at ∼910 K. This could be due to reheating of the ions as they are extracted from the RFQ and accelerated towards the LCR.

5.2 Temperature, CEC-LCR Distance and Power

In this section, the effects of changing the temperature of the beam, the distance between the CEC and the LCR, and the laser power are shown and discussed.

5.2.1 Temperature

The temperature of the atoms as they interact with the laser is expected to affect the widths of the peaks in the resulting hyperfine spectra. Eq. 3.1.3 describes the effects of temperature on the Gaussian contribution to the width of a Voigt profile. Fig 5–3 shows the effects of temperature on a simulated

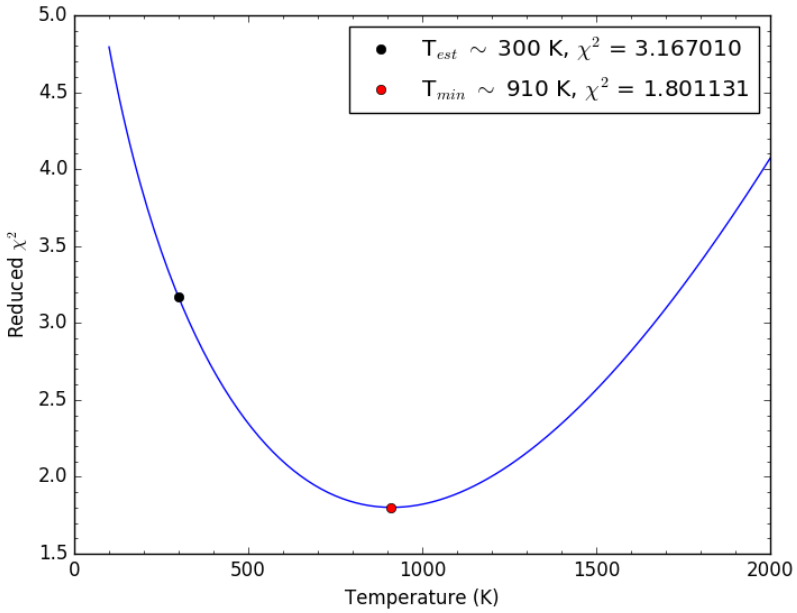

Figure 5–2: The reduced χ^2 statistic as a function of the temperature used in the simulation of a Gallium-69 hyperfine spectrum. The estimated temperature of 300 K is shown, as well as the temperature at which a minimum in the χ^2 value occurs, $\sim$ 910 K.

spectrum of Gallium-69. As the temperature increases, Doppler broadening begins to dominate over the natural linewidth of the peaks and the hyperfine structure of the spectrum is diluted.

5.2.2 CEC-LCR Distance

Eq.4.14 inversely depends on the distance between the CEC and the LCR. The likelihood of an atom reaching the LCR in its original ground state decreases as the CEC-LCR distance increases. Conversely, this likelihood increases as the CEC-LCR distance decreases. Fig 5–4 shows the effects of changing this distance on a simulated Gallium-69 spectrum, for a fixed power of 1.0 mW. Between 0.1 and 1.0 m, there is no discernible difference between the simulated spectra. As the distance increases, optical pumping begins to have a larger effect. At 5 m, the central peak begins to completely dominate the

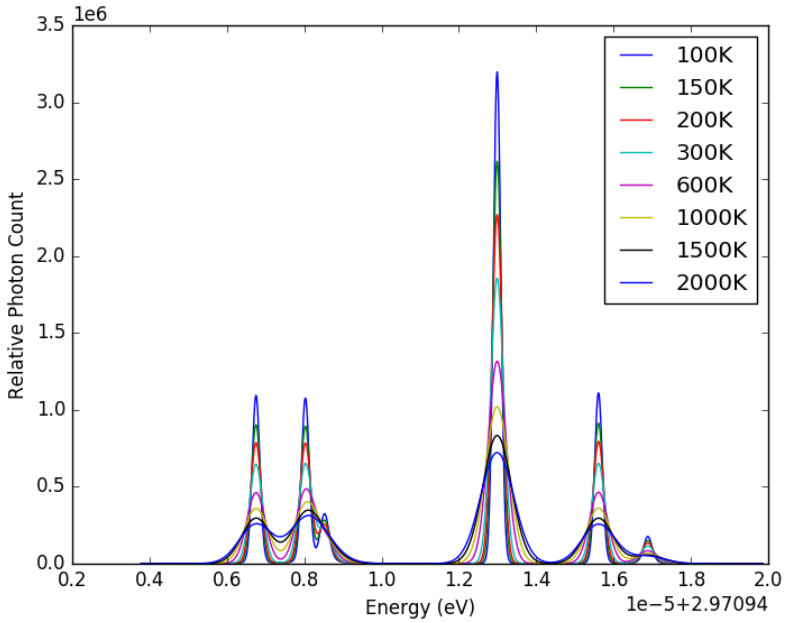

Figure 5–3: The effects of the temperature on the hyperfine spectrum of Gallium-69. As the temperature of the atoms increases, the Doppler contribution to the width of the peaks increases. At sufficiently high temperatures ($\approx 2.0 \times 10^3$ K), the hyperfine structure of the atom begins to smooth out.

spectrum at the expense of the smaller peaks near 1.5 and 4 $\times 10^{-3}$+2.9709512 eV.

5.2.3 Laser Power

The power of the laser is the most important parameter when simulating the effects of optical pumping on a hyperfine spectrum. This sections first shows the behavior of the model as the power is changed. Figures **??** and 5–6 show how a simulated spectrum of Gallium-69 changes as the power of the exciting laser is increased from 1.0 to 100 mW. As the power of the laser is increased, certain transitions become less likely with respect to others, changing the relative intensities of the peaks. At laser powers about 20 mW, the spectrum begins to be dominated by the $F_g = 3 \rightarrow F_e = 2$ transition. At powers above 50 mW, the spectrum is entirely dominated by this transition.

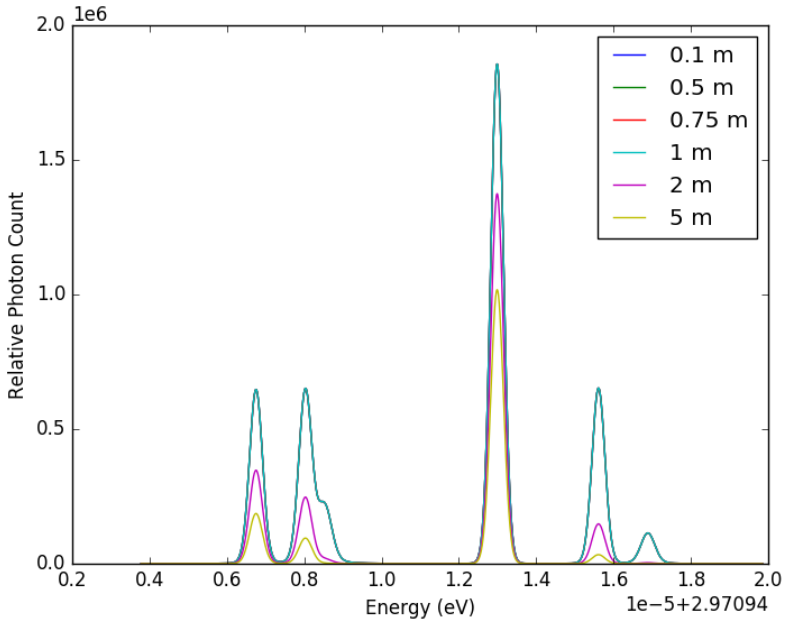

Figure 5–4: The effects of changing the CEC-LCR distance on a simulated spectrum of Gallium-69, for a laser power of 1.0 mW.

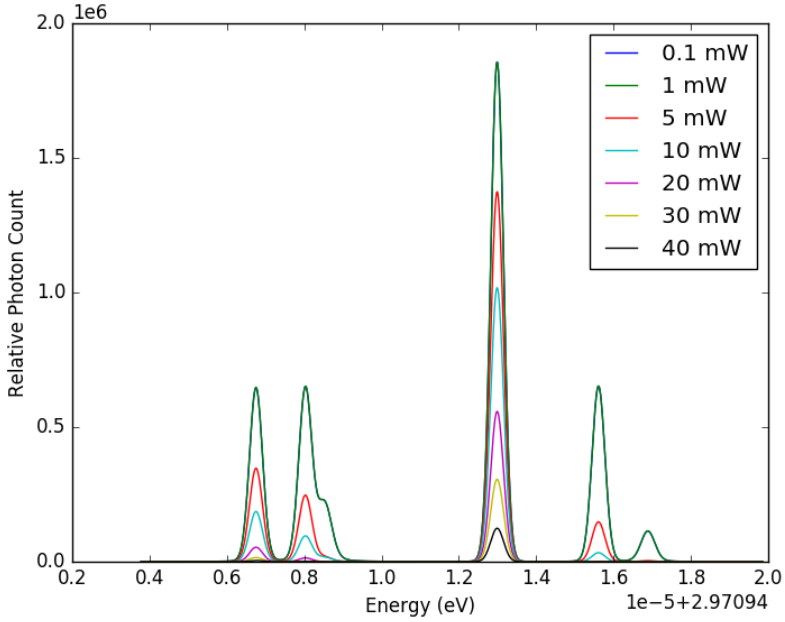

Figure 5–5: The effects of the power of the exciting laser on a simulated Gallium-69 spectrum are shown above for laser powers between 0.1 and 40 mW.

Rubidium-87

In a recent experimental run at TRIUMF, the hyperfine spectrum of Rubidium-87 (I = 1.5, $J_e = 1.5$, $J_g = 0.5$), a level diagram of which is shown

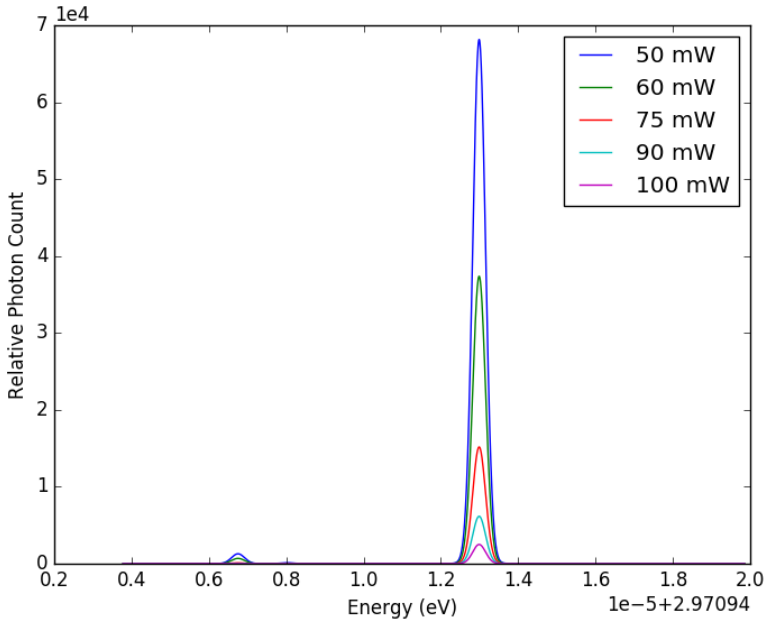

Figure 5–6: Increasing the power of the laser causes optical pumping to have a greater effect on the resulting spectrum. The above shows the simulated spectrum of Gallium-69 for laser powers between 50 to 100 mW.

in Fig. 5–7 was examined as the power of the exciting laser was changed. The experiment was set up in a very similar manner to those described in Chapter 2. However, rather than collecting Rubidium atoms through the collision of protons with a target material, a stable source of Rubidium was used. Below are the results of the run, compared to the spectra predicted by the algorithm described in the previous chapter.

Fig. 5–8 shows the performance of the simulation for laser powers of 4.5 to 18.9 μW. The lack of data between the two groups of peaks is due to the method of scanning used. To reduce the collection time required, only the regions where peaks were expected were scanned. Also shown are the reduced χ^2 values for each comparison. The simulated spectra tend to exaggerate the effects of optical pumping, exemplified by the predicted height of the left-most peak. In each case, this peak is much lower than the corresponding peak in the measured spectrum. This trend continues in Fig. 5–9 and Fig. 5–10 where

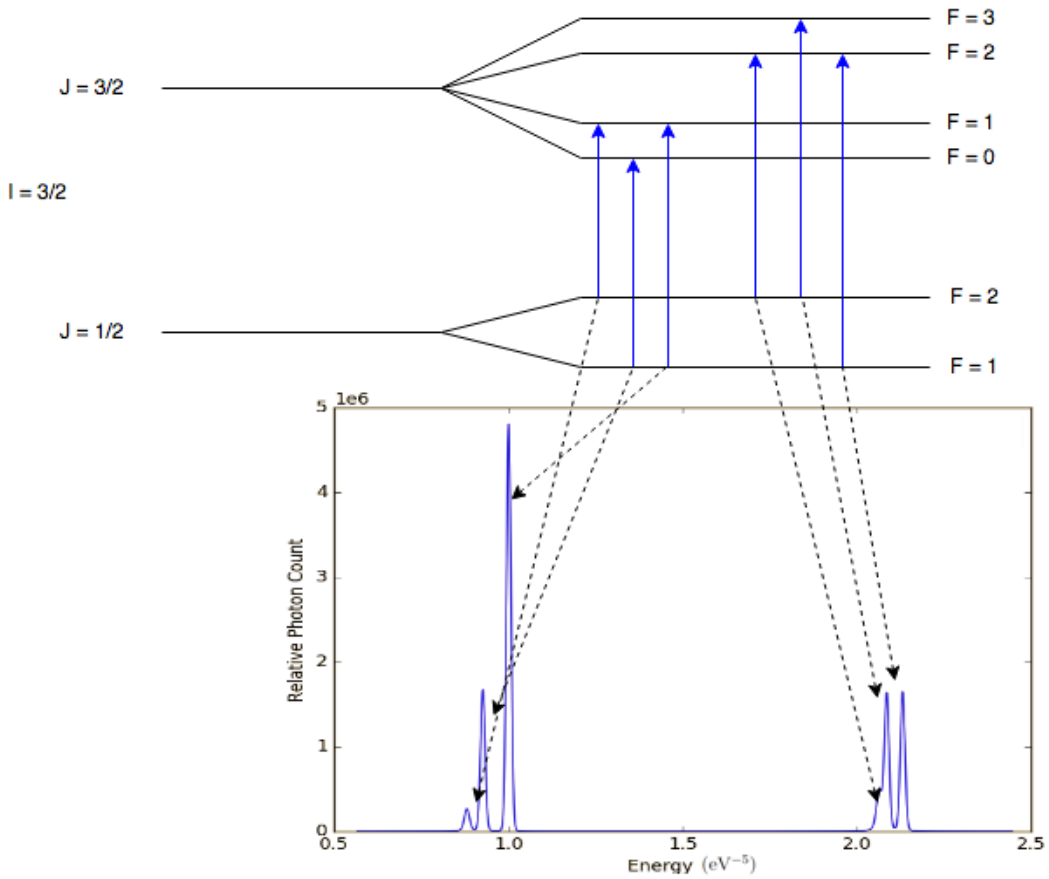

Figure 5–7: Level diagram of Rubidium-87.

the comparison between the simulated and measured spectra are shown, for powers ranging from 22.1 to 36.4 μW and 39.1 to 108.0 μW, respectively. Fig. 5–10d shows the performance of the model when compared to the Rubidium-87 spectra. The reduced χ^2 statistic is reported for each Rubidium spectrum and is plotted as a function of the laser power. As a general trend, the model accuracy decreases as the power increases. Examining the comparisons between the predicted and measured spectra of Rubidium-87, a discrepancy between the expected and measured height of the lowest energy peak, located at $\sim$ 0.75e-5+1.58903 eV, is present across all laser powers, indicating that the model overestimates the effects of optical pumping for this transition ($F_e = 1$,

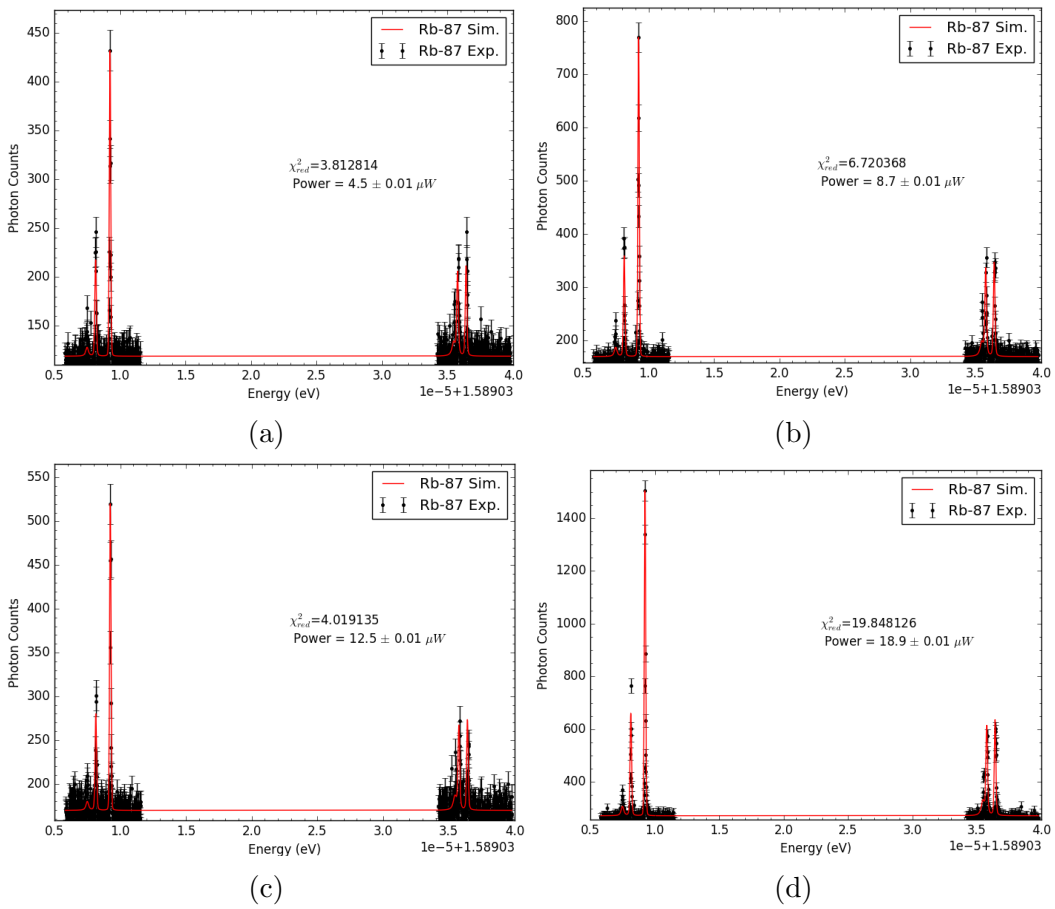

Figure 5–8: Comparison between the simulated (red) and measured (black) hyperfine spectrum of Rubidium-87 for laser power: (a) 4.5 μW (b) 8.7 μW (c) 12.5 μW (d) 18.9 μW.

$F_g = 2$). The most likely culprit for this discrepancy is the assumption that 100% of a the laser power is delivered to the atoms.

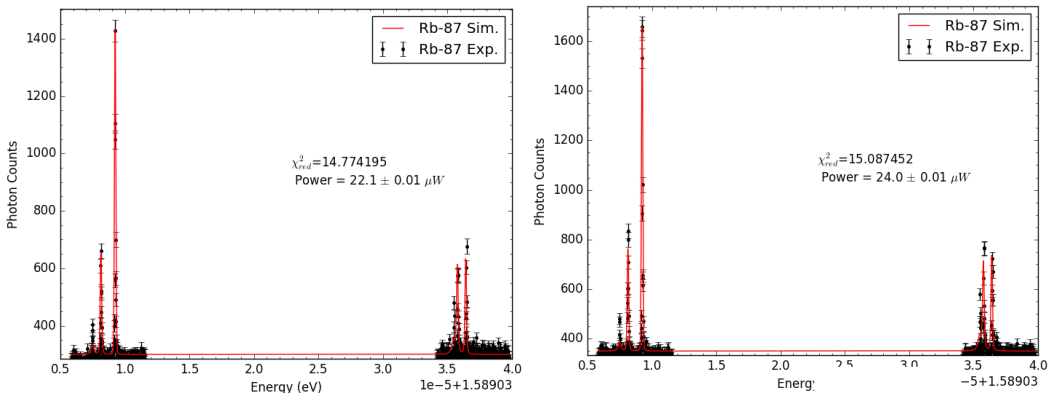

Figure 5–9: Continuing from Fig. 5–8, a comparison between the simulated (red) and measured (black) hyperfine spectrum of Rubidium-87 for laser power: (a) 22.1 μW (b) 24.0 μW (c) 24.4 μW (d) 36.4 μW. Also shown are the reduced χ^2 values for each comparison.

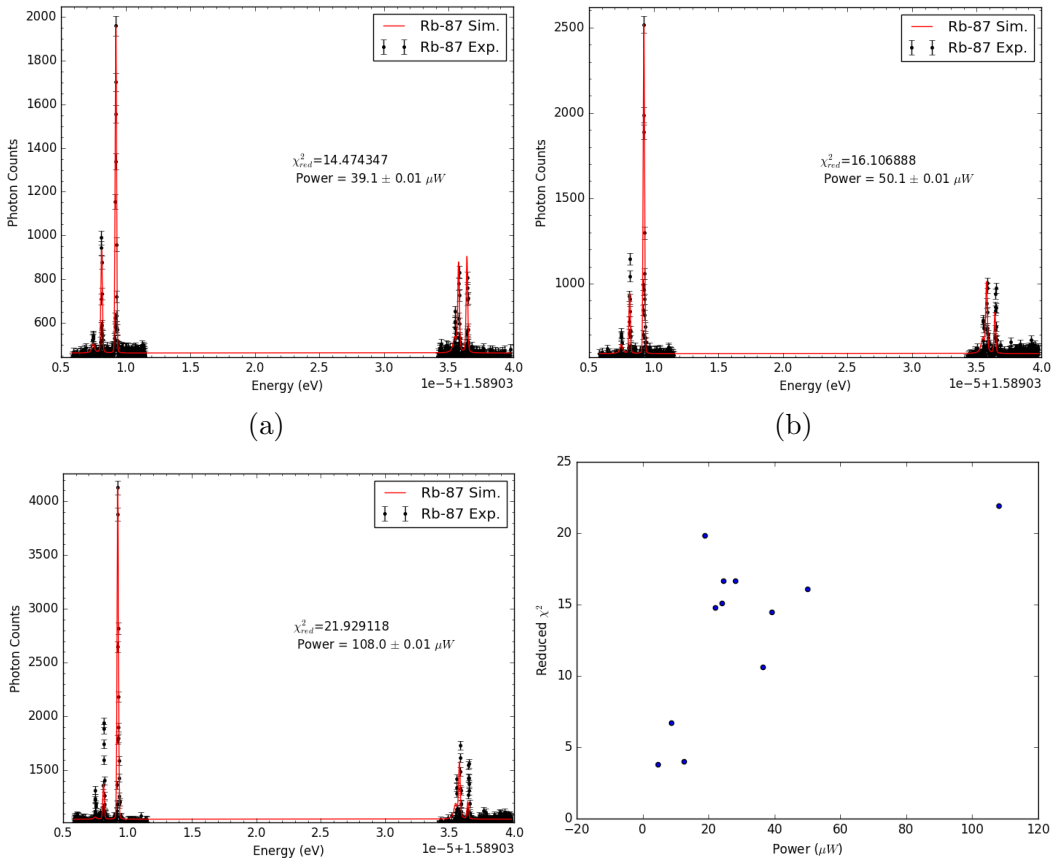

Figure 5–10: The final set of spectra exploring the effect of the laser power on the hyperfine spectrum on Rubidium-87 for laser powers: (a) 39.1 μW (b) 50.1 μW (c) 108.0 μW. Also shown are the reduced χ^2 values for each comparison. (d) shows the reduced χ^2 statistic as a function of the power of the exciting laser for the Rubidium-87 experimental run.

CHAPTER 6
Conclusion

In this work, a brief introduction to collinear laser spectroscopy at TRIUMF was presented, followed by the theoretical background necessary to understand the hyperfine structure of an atom. Then, a treatment of optical pumping as a modification to the Racah intensities was described and then used to simulate the effects of optical pumping on the measured hyperfine spectra of both Gallium-69 and Rubidium-87. The effects of the beam temperature, the experimental geometry and the power of the exciting laser were explored on a simulated Gallium-69 spectrum. Increasing the temperature caused the peak width to increase, while increasing the distance between the CEC and the LCR affected the relative heights of the hyperfine peaks. Increasing the laser power caused the relative peak heights to change. Continuously increasing the laser power led to the complete domination of a single transition, with the other transitions being *pumped out*. When compared to measured Gallium-69 spectra, there was a discrepancy between the assumed beam temperature (300 K) and the temperature that produced most accurate simulation (910 K), possibly caused by an inaccurate estimation of the cooling effects of the RFQ, or a broadening effect caused by the accelerating voltages. When compared Rubidium-87 spectra measured using different laser powers, the simulation consistently underestimated the height of the lowest peak. The discrepancy between the measured and simulated Rubidium-87 spectra seemed to increase with laser power. Given that the simulation was accurate in one case and inaccurate in the other, there is likely some merit in comparing the simulation to different isotopes in future experiments.

Appendices

APPENDIX A
Written Code

```
#This version of the code outputs the likelihood of an
   atom making it to the LCR in the same ground state
   that it started in.


import numpy as n
import math as m
import cmath as cm
import time as ti
from decimal import *
import random as r
import numpy.linalg as lin
from sympy.physics.wigner import wigner_6j, wigner_3j
from scipy.special import wofz
import matplotlib.pyplot as plt




#----------------------INTRO---------------------------



#------------------Preamble
   ------------------------------------
# Important constants
```

```
kB = 8.6173324 * 10**(-5) #eV/K boltzmanns constant
kB_J = 1.38064852e-23#boltzmann constant in J/K
amu = 931.4940954*10**6 #eV/c^2 rest energy of one atomic
    mass unit
amu_kg = 1.66054e-27 #amu in kg
c = 299792458 #m/s speed of light
alpha = 0.0072973525664 #fine structure constant
m_e = 0.5109989461*10**6#eV/c^2 mass of electron
c_e = 1.6021766208*10**(-19) #charge of electron in
   Coulombs
r_e = 2.817*10**(-15)#classical electron radius in m
kB_cc = kB/(c**2)#kB/c^2 boltzmann constant per c^2
hbar = 6.582119514*10**(-16) #reduced planck constant in
   eV*s
h_js = 6.626070040*10**(-34) #planks constant in J s
e_0 = 8.854187817*10**(-6)/(6.242*10**(24)) #vacuum
   perimittivity in Coulombs^2/eV*m
a_0 =  5.29*10**(-11) #bohr radius in m



def GSP(I,J_l):#Returns a random F state for ground state
        Js = n.arange(-J_l,J_l + 1,1)
        Fs = Js + I
        F_mg = 2*Fs+1
        tot = n.sum(F_mg)
        F_mg = F_mg/tot
        F_mat = n.zeros([len(Js),2])
        F_mat[:,0] = Fs
```

```
        F_mat[:,1] = F_mg
        rnum = r.uniform(0,1)
        lower = 0
        for f in n.arange(0,len(Js)):
                upper = lower + F_mat[f,1]
                if rnum == 1:
                        F_state = Fmat[len(Js)-1,0]
                elif lower <= rnum < upper:
                        F_state = F_mat[f,0]
                lower = upper
        return F_state


def Boltz(M,T):#returns random z-velocity from a
   Boltzmann distribution (m/s)
        sig = (kB*T/(2.0*n.pi*M/c**2))**(0.5)
        ran1 = n.random.uniform(0,1)
        ran2 = n.random.uniform(0,1)
        vel = sig*n.sqrt(-2.0*n.log(ran1))*n.cos(2.0*n.pi
           *ran2)
        return vel


def Cauch(mean,gam):
        ran1 = n.random.uniform(0,1)
        cauch = mean + gam*n.tan(n.pi*(ran1-0.5))
        return cauch
```

```
#Define K
def K(F,I,J):
        Kk = F*(F+1.0) - I*(I+1.0) - J*(J+1.0)
        return Kk

#Define Beta
def Beta(K,I,J):
        if I <= 0.5 or J <= 0.5:#check for B coeffs. Set
           to zero if they're not important
                Beta = 0
        else :
                Beta = (3.0*K*(K+1.0)-4.0*I*(I+1.0)*J*(J
                   +1.0))/(8.0*I*(2.0*I-1.0)*J*(2.0*J
                   -1.0))
        return Beta



def E_hf(J,I,F,A,B):#energy of each hyperfine level in eV
   . From allen leary's thesis
        Kk = K(F,I,J)
        E_hfine1 = (hbar*2.0*n.pi)*(0.5*(A*10**6)*Kk)#
           here A is converted to Hz, same for B on the
           next line
        E_hfine2 = (hbar*2.0*n.pi)*((B*10**6)/4.0)*(1.5*
           Kk*(Kk+1.0)-2.0*I*J*(I+1.0)*(J+1.0))/(I*J
           *(2.0*I-1.0)*(2.0*J-1.0))
        ch = m.isnan(E_hfine2)
        if m.isnan(E_hfine2):
```

```
                E_hfine2 = 0
        E = E_hfine1+E_hfine2
        return E


def Rad(N_u,J_u,N_l,J_l):#this function returns the
    radial matrix element for two states in units of a_0
        lw = (N_l,J_l-0.5)
        for ch in n.arange(0,14,1):
                rads = rad_mat[ch]
                if lw in [rads[0]]:
                        break
        if N_u == 2:
                mat_el = rads[1]
        if N_u == 3:
                mat_el = rads[2]
        if N_u == 4:
                mat_el = rads[3]
        if N_u == 5:
                mat_el = rads[4]
        return mat_el



def F(I,J_u,J_l):#returns all the possible transistions
    Fu->Fl J_u, J_l
        J_us = n.arange(-J_u,J_u+1,1)
        J_ls = n.arange(-J_l,J_l+1,1)
        F_us = I + J_us
        F_ls = I + J_ls
        trans = []
```

```
ntrans = 0
for u in F_us:
        for l in F_ls:
                ch = n.abs(u-l)
                if ch == 1:
                        trans.append(u)
                        trans.append(l)
                        trans.append(u-I)
                        trans.append(l-I)
                        amp = (2.0*l+1.0)*(2.0*u
                           +1.0)*(wigner_6j(u,l
                           ,1,J_l,J_u,I))**2
                        trans.append(amp)
                        ntrans = ntrans + 1
                if ch == 0:
                        if u != 0:
                                trans.append(u)
                                trans.append(l)
                                trans.append(n.
                                   abs(u-I))
                                trans.append(n.
                                   abs(l-I))
                                amp = (2.0*l+1.0)
                                   *(2.0*u+1.0)*(
                                   wigner_6j(u,l
                                   ,1,J_l,J_u,I))
                                   **2
                                trans.append(amp)
```

```
                                        ntrans = ntrans +
                                            1
        Ftemp = n.array(trans)
        F = Ftemp.reshape((ntrans,5))
        F[:,4] = F[:,4]/n.sum(F[:,4])
        return F

def mu(N_u,J_u,F_u,F_uz,N_l,J_l,F_l,F_lz,I,q):#compute
    the dipole moment. from eq. 4.33 pg 55 in Laser
    cooling and Trapping (Metcalf)
        rad_el = Rad(N_u,J_u,N_l,J_l)*a_0 #q is the
            photon polarization q = +-1 or 0
        exp = c_e*(-1.0)**(1+(J_u-0.5)+0.5+J_l+J_u+I-F_uz
            )
        sqrt = n.sqrt((2.0*J_u+1.0)*(2.0*J_l+1.0)*(2.0*
            F_u+1.0)*(2.0*F_l+1.0))
        wig6 = wigner_6j((J_u-0.5),J_u,0.5,J_l,(J_l-0.5)
            ,1)*wigner_6j(J_u,F_u,I,F_l,J_l,1)
        wig3 = wigner_3j(F_l,1,F_u,F_lz,q,-F_uz)
        mu = rad_el*exp*sqrt*wig6*wig3
        return mu
def A_calc(J_u,F_u,F_uz,J_l,F_l,F_lz,I,q):#compute the
    dipole moment. from eq. 4.33 pg 55 in Laser cooling
    and Trapping (Metcalf)
        #q is the photon polarization q = +-1 or 0
        exp = c_e*(-1.0)**(1+(J_u-0.5)+0.5+J_l+J_u+I-F_uz
            )
        sqrt = n.sqrt((2.0*J_u+1.0)*(2.0*J_l+1.0)*(2.0*
            F_u+1.0)*(2.0*F_l+1.0))
```

```
        wig6 = wigner_6j((J_u-0.5),J_u,0.5,J_l,(J_l-0.5)
           ,1)*wigner_6j(J_u,F_u,I,F_l,J_l,1)
        wig3 = float(wigner_3j(F_l,1,F_u,F_lz,q,-F_uz))
        A_calc = exp*sqrt*wig6*wig3
        return [A_calc,exp,sqrt,wig6,wig3]

def Dop(v,wn):
        beta = v/c #beta factor
        fact = ((1.0+beta)/(1.0-beta))**(0.5)
        obs = fact*wn
        return obs

def Scatter(gamma,s_0,delta):#scattering rate of photons
   from laser metcalf pg.25
        gamma_prime = gamma*n.sqrt(1.0+s_0)
        scattering_rate = (s_0/(1.0+s_0))*(gamma/2.0)
           /(1.0+(2.0*delta/gamma_prime)**2)
        return scattering_rate

def Lorentz(xdata,cent,gamma):
        Lor = (1.0/n.pi)*(gamma/((xdata-cent)**2+gamma
           **2))
        return Lor

def gaussian(xdata,cent,sig):
        Gauss = n.exp(-(xdata-cent)**2/(2*sig**2))/(sig*n
           .sqrt(2.0*n.pi))
        return Gauss
```

```
def realvoigt(xdata,cent,f_g,f_l):
        z = (xdata-cent+1j*f_l)/(f_g*n.sqrt(2*n.pi))
        wof = wofz(z)
        voigt = wof.real/(f_g*n.sqrt(2*n.pi))
        return voigt


def pseudovoigt(xdata,cent,f_g,f_l):
        f = (f_g**5+2.69269*f_g**4*f_l+2.42843*f_g**3*f_l
           **2+4.47163*f_g**2*f_l**3+0.07842*f_g*f_l**4+
           f_l**5)**(1.0/5)
        #eta =1.0 - n.abs(1-(1.36606*(f_l/f)-0.47719*(f_l
           /f)**2+0.11116*(f_l/f)**3))
        #eta=1
        eta = 1.36606*(f_l/f)-0.47719*(f_l/f)
           **2+0.11116*(f_l/f)**3
        pseudovoigt = (eta*Lorentz(xdata,cent,f_l/2.0)
           +(1.0-eta)*gaussian(xdata,cent,f_g/2))
        return pseudovoigt,eta

def voigt(xdata,amp,cent,sig,ep):#define the voigt peak.
   If ep is less than 0 or greater than 1, mess up the
   profile
    x = xdata
    C = cent
    S = sig
    A = amp
    E = ep
```

```
    Sg = S/n.sqrt(2*n.log(2))
    vmodel = (A*(1.0-E)/(Sg*n.sqrt(2.0*n.pi)))*n.exp(-(x-
       C)**2/(2.0*Sg**2))+ ((E*A)/(n.pi))*(S)/((x-C)**2+S
       **2)
    if 0>E or 1<E:
        vmodel = vmodel + 50000
    return vmodel



#-----------------------Inputs
   -------------------------------------


v_c = raw_input('Use the same parameter vector?(y/n)')#
   makes it easier to rerun things

#v_c = 'y'
if v_c in ['n']:
        mss = float(raw_input('Isotope mass (AMU):'))#get
            mass of isotope
        Z = float(raw_input('Z (# of protons):'))#get
           charge of nucleus
        J_l = float(raw_input('Lower J state:'))#get
           lower J state of transition
        J_u = float(raw_input('Upper J state:'))#get
           upper J state of transition
        I = float(raw_input('Nuclear spin:'))#get nuclear
            spin of isotope
```

```
        gamma_e = float(raw_input('Experimental decay
            rate of fine structure transition (Hz):'))
        A_u = float(raw_input('Upper A coefficient (MHz):
            '))#hyperfine coefficients
        A_l = float(raw_input('Lower A coefficient (MHz):
            '))
        B_u = float(raw_input('Upper B coefficient (MHz):
            '))
        B_l = float(raw_input('Lower B Coefficiet (MHz):'
            ))
        T = float(raw_input('Beam Temperature (K):'))#get
             beam temperature
        l_wn = float(raw_input('Laser wavenumber (cm^(-1)
            ):'))#get laser wavelength
        l_p = float(raw_input('Laser Power (mW):'))#get
            laser power
        wn_fs = float(raw_input('Fine Structure
            transition wavenumber (cm^(-1)):'))
        d = float(raw_input('Distance between CEC and LCR
            (m):'))#distance over which optical pumping
            is problematic
        FILENAME = str(raw_input('Experimental file (if
            none, then write n)'))
        vec = [mss,Z,J_l,J_u,I,gamma_e,A_u,A_l,B_u,B_l,T,
            l_wn,l_p,wn_fs,d,FILENAME]


if v_c in ['y']:
        mss = float(vec[0])
```

```
        Z = float(vec[1])
        J_l = float(vec[2])
        J_u = float(vec[3])
        I = float(vec[4])
        gamma_e = float(vec[5])
        A_u = float(vec[6])
        A_l = float(vec[7])
        B_u = float(vec[8])
        B_l = float(vec[9])
        T = float(vec[10])
        l_wn = float(vec[11])
        l_p = float(vec[12])
        wn_fs = float(vec[13])
        d = float(vec[14])
        FILENAME = vec[15]

m_is = amu*int(mss) #mass of the isotope
m_is_kg = amu_kg*int(mss)
En_fs = hbar*n.pi*2*c*10**2*(wn_fs)#energy in eV of fine
   structure
prefact = 3.0*n.pi*e_0*hbar*c**3*gamma_e/c_e**2

#Determine lifetimes and widths of each transition

F_t = F(I,J_u,J_l)#get the transitions and transition
   amplitudes
n_tr = F_t.shape[0]#number of transitions
n_par = F_t.shape[1]#number of parameters in F_t
```

```
F_n = n.zeros((n_tr,15))#create new matrix with extra
   columns of Photon energy, Energy width, lifetime,
   saturation intensity, saturation parameter
F_n[0:n_tr,0:n_par] = F_t #put in original F_t

#the next section will be filling F_n with the relevant
   quantities, up until A


A_vec = n.zeros((n_tr))
omeg_vec = n.zeros((n_tr))
#count = 0
for k in n.arange(0,n_tr,1):
        A_calc_int=0
        A_calc_tot = 0
        #first, photon energy
        f_u = F_n[k,0]#get upper F state
        f_l = F_n[k,1]#get lower F State
        f_u_en =  E_hf(J_u,I,f_u,A_u,B_u) #get energy of
           upper state knowing the fine structure energy
        f_l_en =  E_hf(J_l,I,f_l,A_l,B_l) #get energy of
           lower state knowing the fine structure energy
        del_en = f_u_en-f_l_en + En_fs
        F_n[k,4] = del_en #get energy difference in eV
           and store it
        omeg = del_en/hbar #angular frequency in Hz
```

```
        #next, get mean lifetime of decay. To do this, we
            need to compute A for each (f_uz,f_lz,q) This
            is spontaneous emission
        A_calc_int = 0
        A_calc_tot = 0
        for fuz in n.arange(-f_u,f_u+1,1):#for each
           projection on z axis of top F state
                for flz in n.arange(-f_l,f_l+1):#for each
                    projection on z axis of lower F state
                        for q in [-1.0,0,1.0]:
                                A_calc_int = n.abs(A_calc
                                   (J_u,f_u,fuz,J_l,f_l,
                                   flz,I,q)[0])
                                A_calc_tot = A_calc_tot+
                                   A_calc_int
        A_vec[k] = A_calc_tot
        omeg_vec[k] = omeg

R_exp = (prefact*n.sum(1.0/(A_vec**2*omeg_vec**3.0)))
   **(0.5)

for k in n.arange(0,n_tr,1):

        mutot = R_exp*c_e*A_vec[k]
        dec_r = (omeg_vec[k]**3)*(mutot**2)/((3.0*n.pi)*
           e_0*hbar*c**3)/10#decay rate in Hz
        tau = 1.0/dec_r
        spread = hbar/(2*tau)
        F_n[k,5] = spread #input energy spread in eV
```

```
        F_n[k,6] = tau #input lifetime in seconds
        F_n[k,7] = F_t[k,4]
        wl_fs = 2.0*n.pi*hbar*c/En_fs
        wl = 2.0*n.pi*hbar*c/del_en #transition
           wavelength in meters
        I_s =  n.pi*h_js*c/(3.0*(wl**3.0)*tau) #compute
           saturation intensity pg. 25 in Metcalf, in W
        F_n[k,8] = I_s
        F_n[k,9] = (l_p)/(I_s/10.0) #compute on resonance
            saturation parameter pg. 25 in metcalf
        #compute the velocity of the atoms on resonance
        e_trans = F_n[k,4]#transition energy
        f_trans = e_trans/(hbar*2.0*n.pi)#transition
           frequency
        f_init = c*(l_wn*100)#initial frequency in hz
        v_trans = c*((f_trans**2-f_init**2)/(f_trans**2+
           f_init**2))
        F_n[k,10] = n.abs(v_trans) #speed of the atom
           necessary for resonance

#next, evaluate the likelihood that an atom in gs G will
   come back to that state after being excited
F_n_shape=F_n.shape
for k in n.arange(0,n_tr,1):
        F_n_temp = []
        trans = 0
        gs = F_n[k,1]#get the ground state
        es = F_n[k,0]#get the excited state
        for kk in n.arange(0,n_tr,1):
```

```
        if F_n[kk,0] == es:
                F_n_temp.append(F_n[kk,:])#get
                    all the transitions with es as
                     excited state
                trans = trans+1
F_n_temp = n.reshape(F_n_temp,(trans,F_n_shape
    [1]))#reshape the array
decay_rates = 1.0/F_n_temp[:,6]
tot_decay_rate = n.sum(decay_rates)
decay_rates_norm = decay_rates/tot_decay_rate
for kkk in n.arange(0,len(decay_rates),1):#find
    the one transition that allows for the same gs
        if F_n_temp[kkk,1]==gs:
                prob_of_og=decay_rates_norm[kkk]#
                    likelihood of returning to og
                    ground state
                F_n[k,11] = decay_rates_norm[kkk]
                    #store likelihood of returning
                     to og ground state
                scatter_res = Scatter(1.0/F_n[k
                    ,6],F_n[k,9],0)#get scattering
                     rate on resonance
                F_n[k,12]=scatter_res#store
                    scattering rate on resonance
                tot_time = F_n[k,6]+1.0/
                    scatter_res#get total
                    transition time = scattering
                    time + lifetime
```

```
                        num_trans = m.floor((d/F_n[k,10])
                            /tot_time)#total number of
                            transitions rounded down
                        F_n[k,13] = num_trans#store
                            number of transitions
                        prob = prob_of_og**(num_trans)#
                            likelihood of finding og gs
                            when you enter LCR
                        F_n[k,14] = prob#store the above
                            prob


#now start plotting what a regular spectrum should look
    like


xdata = n.arange(n.min(F_n[:,4])*0.999999,n.max(F_n[:,4])
    *1.000001,1e-8)

spec_sum = n.zeros((len(xdata),))
spec_int = 0
amp=1
#print vec[12]
#print vec[10]
for spec in n.arange(0,n_tr,1):
        gamma_stim_cal = (1.0/((1.0/(F_n[spec,6])))*n.
            sqrt(1.0+I/F_n[spec,8]))
        gamma_stim = 1/(1.0/((1.0/gamma_e))*n.sqrt(1.0+I/
            F_n[spec,8]))
```

```
#gamma_stim_used = 1/(n.pi*2*(1/gamma_e))*hbar
   *2.0*n.pi*n.sqrt(1.0+I_s/F_n[spec,8])
boltz_FWHM = F_n[spec,4] * (8.0*kB_J*T*n.log(2)/(
   m_is_kg*c**2))**(0.5)
boltz_HWHM_rel = (1.0/8.0)*(2.0*kB_J*T*n.log(2)/(
   m_is_kg*c**2))**(0.5)
spec_int = F_n[spec,14]*F_n[spec,7]*realvoigt(
   xdata,F_n[spec,4],boltz_HWHM_rel,
   gamma_stim_cal)#plot the peak weighed by the
   chances of it not being pumped
print boltz_HWHM_rel
print gamma_stim_cal
#print F_n[spec,5]*n.sqrt(1.0+I/F_n[spec,8])
#print F_n[:,14]
spec_sum=spec_sum+spec_int
```

REFERENCES

[1] Albert A. Michelson. On the application of interference methods to spectroscopic measurements.–ii. *The London, Edinburgh, and Dublin Philosophical Magazine and Journal of Science*, 34(208):280–299, 1892.

[2] W. Pauli. Zur frage der theoretischen deutung der satelliten einiger spektrallinien und ihrer beeinflussung durch magnetische felder. *Naturwissenschaften*, 12(37):741–743, Sep 1924. ISSN 1432-1904.

[3] Klaus-Peter Lieb. Theodor Schmidt and Hans Kopfermann – Pioneers in Hyperfine Physics. *Hyperfine Interactions*, 136(3):783–802, No 2001.

[4] A. Voss, T. J. Procter, O. Shelbaya, P. Amaudruz, F. Buchinger, J. E. Crawford, S. Daviel, E Mané, M. R. Pearson, and W. Al Tamimi. The Collinear Fast Beam laser Spectroscopy (CFBS) experiment at TRIUMF. *Nuclear Instruments and Methods in Physics Research Section A-Accelerators Spectrometers Detectors and Associated Equipment*, 811: 57–69, 2016. ISSN 0168-9002.

[5] Fujia Yang and Hamilton Joseph H. *Modern atomic and nuclear physics*. World Scientific, 2010.

[6] T. Procter et al. Nuclear mean-square charge radii of $^{63,64,66,68-82}$ga nuclei: No anomalous behavior at $n = 32$. *Phys. Rev. C*, 86, Sep 2012.

[7] Thomas Procter. *New Techniques of Laser Spectroscopy on Exotic Isotopes of Gallium and Francium*. PhD thesis, The University of Manchester, 2013. Unpublished.

[8] Carlos A. Bertulani. *Nuclear physics in a nutshell*. Princeton University Press, 2007.

[9] Wolfram MathWorld. *http://mathworld.wolfram.com/Spheroid.html*, 2017.

[10] C. Kittel and H. Kroemer. *Thermal Physics*. W. H. Freeman, 1980.

[11] L.D. Landau and E.M Lifshitz. *The Classical Theory of Fields*. Course of theoretical physics. Butterworth-Heinemann, 1975.

[12] G.K. Wertheim, M.A. Butler, K.W. West, and D.N.E. Buchanan. Determination of the gaussian and lorentzian content of experimental line shapes. *Review of Scientific Instruments*, 45:1369, 1974.

[13] H.J Metcalf and P. van der Straten. *Laser Cooling and trapping*. Springer-Verlag New York, 1999.

[14] John S. Townsend. *A Modern Approach to Quantum Mechanics*. Univ Science Books, 2012.

[15] D. Morin. *Introduction to Classical Mechanics*. Cambridge University Press, 2008.

[16] G. J. Farooq-Smith and A. R. et al. Vernon. Probing the $_{31}$Ga ground-state properties in the region near $Z = 28$ with high-resolution laser spectroscopy. *Phys. Rev. C*, 96:044324, Oct 2017.